Atomic scale modeling of grain boundaries: the role of impurities in copper

Thomas Cnops

Promotoren: prof. dr. Stefaan Cottenier, prof. dr. ir. Kim Verbeken

Masterproef ingediend tot het behalen van de academische graad van
Master in de ingenieurswetenschappen: materiaalkunde

Vakgroep Toegepaste Materiaalwetenschappen
Voorzitter: prof. dr. ir. Joris Degrieck
Faculteit Ingenieurswetenschappen en Architectuur
Academiejaar 2012-2013

UNIVERSITEIT
GENT

This work has been performed at the Center for Molecular Modeling,
in collaboration with the Department of Materials Science and Engineering.

Preface

I would like to thank my supervisors, prof. Cottenier and prof. Verbeken for their feedback, effort and mainly for their patience that made this dissertation possible. I would also like to thank Kurt Lejaeghere and Michael Sluydts for their quick replies every time I faced a minor, major or urgent crisis. Furthermore, I want to express my gratitude for the excellent workspace I received at the Center for Molecular Modeling. I enjoyed working there, not only because of the infrastructure, but also because of the people I met.

Of course I also want to mention my friends and fellow students. I would never have made it this far without them.

Thomas Cnops

Atomic scale modeling of grain boundaries: the role of impurities in copper

Thomas Cnops

Supervisors: prof. dr. Stefaan Cottenier, prof. dr. ir. Kim Verbeken

Master dissertation submitted to obtain the academic degree of
Master of Science in Materials Engineering

Department of Materials Science and Engineering
Head of Department: prof. dr. ir. Joris Degrieck

Faculty of Engineering and Architecture
Academic year 2012-2013

Summary

Grain boundaries are generally enriched in impurities compared to the bulk of the material due to a process known as grain boundary segregation. The locally altered concentrations in the grain boundaries can have profound impact on the properties of the material as a whole. In this work the driving force behind this segregation, the grain boundary segregation energy, is investigated using atomic-scale Density Fucntional Theory (DFT) calculations.

The Σ9 grain boundary in copper with phosphorus as a segregating atom is chosen as a model. Using the lattice parameter obtained by a Birch-Murnaghan fit, a supercell is constructed containing a grain boundary. As the supercell is smaller than the interaction range of the grain boundaries, only some atoms are allowed to relax in order to retain an environment resembling bulk copper. Those atoms further from the grain boundaries are fixed in their bulk configuration.

The total energy is calculated for systems containing phosphorus atoms in an infinite bulk environment, in a bulk-like environment between grain boundaries, and in several places on the grain boundary itself. From these values, the segregation energy is calculated. A relationship is found between the segregation energy for a particular site and the distance to the nearest neighbors.

The resulting segregation energy agrees with expectations and the errors incurred during the calculations appear to be on the order of ten percent. The followed method could thus be applied for a systematic investigation of the relationship between atomic configuration in the grain boundary and segregation energy.

Keywords — grain boundary, segregation energy, DFT, atomic scale

Modelleren van korrelgrenzen op atomaire schaal: de rol van onzuiverheden in koper

Thomas Cnops

Promotoren: prof. dr. Stefaan Cottenier, prof. dr. ir. Kim Verbeken

Masterproef ingediend tot het behalen van de academische graad van
Master in de ingenieurswetenschappen: materiaalkunde

Vakgroep Toegepaste Materiaalwetenschappen
Voorzitter: prof. dr. ir. Joris Degrieck

Faculteit Ingenieurswetenschappen en Architectuur
Academiejaar 2012-2013

Samenvatting

Korrelgrenzen zijn doorgaans rijker in onzuiverheden dan de bulk van het materiaal wegens een proces dat bekend staat als korrelgrenssegregatie. De lokaal gewijzigde concentratie in de korrelgrenzen kan een ernstige invloed hebben op de eigenschappen van het volledige materiaal. In dit werk wordt de drijvende kracht achter deze segregatie, de zogenaamde segregatie energie, onderzocht met Density Functional Theory (DFT) berekeningen.

De Σ9 korrelgrens in koper met fosfor als segregerend element werd als model gekozen. De roosterparameter werd bekomen door een Birch-Murnaghan fit uit te voeren. Met deze roosterparameter werd een supercel geconstrueerd. Omdat deze cel kleiner is dan de afstand waarover een korrelgrens het kristal verstoort, werden niet alle atomen gerelaxeerd opdat het gebied tussen de korrelgrenzen op bulk koper zou blijven lijken. De atomen verder van de korrelgrens werden vastgezet in de atomaire configuratie van bulk koper.

De totale energie werd berekend voor systemen met fosfor in een oneindige bulkfase, in een bulkachtige omgeving tussen de korrelgrenzen en in vijf plaatsen aan de korrelgrens. Uit deze waarden werd de segregatie energie berekend. Er werd een verband gevonden tussen de segregatie energie voor een bepaalde plaats op de korrelgrens en de afstand tot de dichtstbijzijnde buur.

De resulterende segregatie energie komt overeen met de verwachtingen en de fouten die opgelopen werden tijdens de berekening zijn van de orde van tien procent. De gebruikte methode kan dus toegepast worden voor een systematisch onderzoek naar het verband tussen een atomaire configuratie in de korrelgrens en de segregatie energie.

Trefwoorden — korrelgrens, segregatie energie, DFT, atomaire schaal

Atomic scale modeling of grain boundaries: the role of impurities in copper

Thomas Cnops

Supervisors: prof. dr. Stefaan Cottenier, prof. dr. ir. Kim Verbeken

Abstract — **The presence of impurities in grain boundaries has the potential to severely affect the properties of the bulk material. The impurity concentration in the grain boundary is often amplified by grain boundary segregation. The driving force behind grain boundary segregation, the segregation energy, depends on the atomic configuration of the grain boundary. In this work, the segregation energy has been calculated for a specific system: phosphorus in a modified $(2\bar{2}1)$ Σ9 [110] copper grain boundary. The agreement between the calculated and the experimental values indicate that the followed method gives good results and can be readily applied to other systems.**

Keywords — **grain boundary, segregation energy, DFT, atomic scale**

I. Introduction

It is often surprising how much influence alloying elements can have on the properties of a material, even if they are present in minute concentrations. The archetypical example is the iron-carbon system. The presence of a few tenths of a percent of carbon by weight is all that separates the –for structural applications at least– useless pure iron from the ubiquitous steel. The adverse effects of some impurities can be equally impressive. The presence of 45 ppm bismuth in copper can lower the stress needed for fracture by more than a factor of five for bicrystals.[1]

Grain boundaries play a critical role in such situations. Unlike other defects, grain boundaries form a continuous network throughout polycrystalline materials and as such they hold the material together. Failure of the grain boundaries implies failure of the bulk material. Additionally, grain boundaries are crystallographic defects. Impurities near a defect are often energetically favored compared to impurities in bulk. As such, a driving force exists that enriches grain boundaries in impurities well above the average concentration. This driving force is the grain boundary segregation energy: the energy gain (or loss) when an impurity moves from the bulk crystal to a grain boundary..

The segregation energy depends on the exact nature of the grain boundary[2]. Unfortunately, the nature of this dependence is out of reach of the experiment. Both aspects of the problem are problematic: measuring the segregation energy and determining the exact atomic configuration at the grain boundary. Therefore, alternatives to experimentation must be explored. Ab-initio calculations offer such an alternative. Starting from well-known physical laws, including the postulates of quantum mechanics, it is in principle possible to model any system on an atomic scale, exactly the relevant scale for grain boundary segregation. For this work Density Functional Theory (DFT) is used, an ab-initio method.

II. The modeled system

For the evaluation of properties of solids, DFT generally uses periodic boundary conditions. This limits the possible grain boundaries, as they must have a small repeating unit. Most grain boundaries encountered in practice do not have such a small repeat unit, they are often called random grain boundaries.

In order to choose a model system that resembles random grain boundaries as much as possible, the grain boundary energy is compared. It is assumed that boundaries with similar energies will have similar behavior. Random grain boundaries generally have a higher energy than the special grain boundaries that can be modeled with DFT. A special grain boundary with a relatively high energy is the modified $(2\bar{2}1)$ Σ9 [110] boundary, yet the boundary does not have such a high energy that it does not occur in practice.[3] The boundary is modified because the standard Σ9 boundary contains two atoms that are very close together, as shown in Figure 1, which is not a realistic configuration.

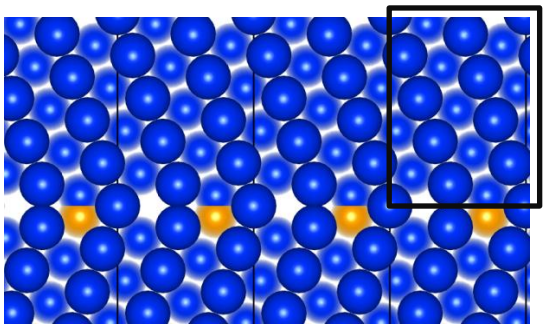

Figure 1: A view along the [110] axis of the Σ9 grain boundary. The thin black lines mark the repeat units. The fuzzy atoms are in a different plane than the page. In the modified Σ9 grain boundary, the yellow atoms are removed. The black rectangle is an outline of Figure 2.

DFT can also model only a limited number of atoms, a hundred atoms in one unit cell is a large system. Thus, the lowest concentration for any impurity is 1 at%. To avoid problems with supersaturation, phosphorus was chosen as an impurity, since it has an appreciable solubility in copper.

III. Results

A. *Validation of the model system*

Two intermediate results are important checks for the quality of the calculations.

The calculated grain boundary energy for the modified $(2\bar{2}1)$ Σ9 [110] is 837mJ/m^2. This value is ~10% higher than typical experimental values, and shows good agreement with other ab initio calculations on special grain boundaries[4, 5].

Due to the limited size of the repeat unit in DFT, it is also worthwhile to check how the influence of the grain boundary is felt throughout the cell. This can be done by comparing valence electron densities between a cell with a grain boundary and a cell without a grain boundary. In Figure 2 the isosurfaces of this difference are plotted in a unit cell.

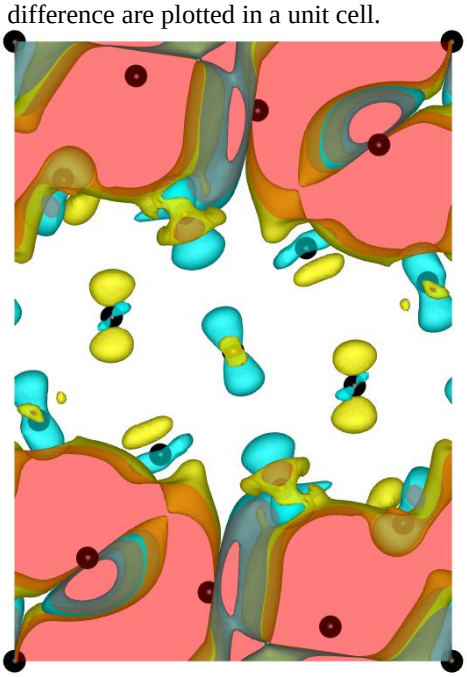

Figure 2: Isosurfaces of density difference of ± 10^{-3} electrons per nm^3. The red areas are intersections of isosurfaces with the viewing plane, the black spheres represent atom positions. The grain boundaries are located on the top and bottom edges of the figure.

Although the influence of the grain boundary is clearly felt throughout the unit cell, there is a relatively large area where the difference in electron densities is less than 10^{-3} electrons per nm^3. For comparison, the average valence electron densities are 864 and 915 electrons per nm^3 for the boundary and bulk cell respectively, although this concentration is mainly concentrated around the nuclei.

Further indication that the grain boundary cell contains a bulk-like environment is given by the comparison made in Table 1.

Table 1: Energy expended when a free phosphorus atom and a bound copper atom exchange state.

Bulk-like	-1.256 eV/atom
True bulk	-1.241 eV/atom

The difference is 0.015 eV/atom or 1450 J/mol. For comparison: a low segregation energy is typically above 40 kJ/mol, around 0.4 eV/atom[5].

B. *Segregation energy*

The segregation energy was calculated for four substitutional positions on the grain boundary and one interstitial. The results in Table 2 have the convention that a negative segregation energy implies that a position at the grain boundary is more favorable than one in bulk.

Table 2: Segregation energies for several positions on the grain boundary

Substitutional 1	-0.588 eV/atom
Substitutional 2	-0.466 eV/atom
Substitutional 3	+0.049 eV/atom
Substitutional 4	-0.175 eV/atom
Interstitial	+0.348 eV/atom

Position one and two have typical segregation energies, and will cause noticeable segregation levels. Position four will contribute much less to the segregation and the other two sites will not contribute. It can also be noted that position one and two have closer neighboring copper atoms than position three and four. The hole containing the interstitial phosphorus atom appears to be too small.

Additionally, after relaxation, all neighbors come closer simultaneously. Meaning that the shortening of the phosphorus-copper distances happens at the expense of copper-copper distances.

IV. Accuracy assessment

Perhaps even more important than the calculated values themselves is an estimate of the uncertainty on the result. Errors come from two sources: numeric errors stemming from the calculations themselves and intrinsic errors due to the modeled system.

A. *Uncertainty on calculations*

The final segregation energy is the difference of the energy of a cell with a phosphorus atom in the bulk-like environment and a cell with a phosphorus atom close to the grain boundary. Although many separate aspects determine the errors of a calculation, it was

found that one source dominates. When the number of terms in the plane wave series used to approximate the electron density was increased, the total energy of the system fluctuates. At the used cut-off these fluctuations had a magnitude of 0.01 eV, four times larger than other sources.

B. Errors from the model and method

Two potential sources of error in the model have already been identified in section III.A: the discrepancy between a true random grain boundary and the modified Σ9 grain boundary and the difference between the bulk-like environment in the grain boundary cell and that of a true bulk cell.

Additional errors are caused by the periodicity of the system. The impurities and especially the grain boundaries are repeated very close together and will interact. Also, the segregation energy is calculated for a finite concentration jump, either the grain boundary contains an atom or it contains none at all, while the real segregation energy should depend on an infinitesimal concentration difference. Lastly, the DFT method inherently contains several approximations in order to make calculations feasible.

Estimating the magnitude of these errors is difficult. Only comparison with the experiment can be used to estimate the error due to the finite accuracy of DFT. The error of 0.015 eV in Table 1 is an indication that the influence of the periodicity is limited. Since phosphorus has a reasonable solubility in copper, it is also expected that interaction between phosphorus is limited for the concentrations under consideration.

V. CONCLUSION

The grain boundary segregation energy has been calculated for a modified Σ9 grain boundary. The result lies within expectations and should be at least an order of magnitude larger than the uncertainty on the calculations and the model.

Peculiar behavior has also been observed when the phosphorus atoms in the grain boundary were allowed to relax. Both positions where neighbors were closer and further, all neighboring distances were shortened simultaneously, rather than optimizing some distances at the cost of others. Due to the insight obtained, the followed procedure can be called successful and thus it can be reused in the future for similar calculations.

ACKNOWLEDGEMENTS

This work was carried out using the Stevin Supercomputer Infrastructure at Ghent University, funded by Ghent University, the Hercules Foundation and the Flemish Government – department EWI. Crystallographic data was obtained from the Crystallographic Open Database[6]. The author would also like to acknowledge the Center for Molecular Modeling and its people for their advice and support.

REFERENCES

[1] Li, G.H. and L.D. Zhang, R*elationship between misorientation and bismuth induced embrittlement of 001 tilt boundary in copper bicrystal.* Scripta Metallurgica Et Materialia, 1995. **32**(9): p. 1335-1340.

[2] Alber, U., H. Mullejans, and M. Ruhle, *Bismuth segregation at copper grain boundaries.* Acta Materialia, 1999. **47**(15-16): p. 4047-4060.

[3] Ikeda, K.-i., et al., *Grain boundary structure of ultrafine grained pure copper fabricated by accumulative roll bonding.* Materials Transactions, 2008. **49**(1): p. 24-30.

[4] Hu, J.R., et al., *HRTEM investigation of the multiplicity of Sigma=9 01-1 /(122) symmetric tilt grain boundary in Cu.* Materials Chemistry and Physics, 2002. **74**(3): p. 313-319.

[5] Lozovoi, A.Y., A.T. Paxton, and M.W. Finnis, *Structural and chemical embrittlement of grain boundaries by impurities: A general theory and first-principles calculations for copper*. Physical Review B, 2006. **74**(15).

[6] Grazulis, S., et al., *Crystallography Open Database (COD): an open-access collection of crystal structures and platform for world-wide collaboration.* Nucleic Acids Research, 2012. **40**(D1): p. D420-D427.

Modelleren van korrelgrenzen op atomaire schaal: de rol van onzuiverheden in koper

Thomas Cnops

Begeleiders: prof. dr. Stefaan Cottenier, prof. dr. ir. Kim Verbeken

Abstract — **De aanwezigheid van onzuiverheden in korrelgrenzen kan mogelijk de mechanische eigenschappen van het bulkmateriaal sterk verzwakken. De concentratie aan onzuiverheden in de korrelgrenzen wordt vaak vergroot door korrelgrenssegregatie. De segregatie energie, de drijvende kracht achter deze korrelgrenssegregatie, hangt af van de atomaire configuratie van de korrelgrens. In dit werk werd de segregatie energie voor een specifiek systeem onderzocht: fosfor in een $(2\bar{2}1)$ Σ9 [110] korrelgrens in koper. De overeenkomst tussen de berekende en experimentele waarden suggereert dat de gevolgde methode goede resultaten geeft en toegepast kan worden op andere systemen.**

Trefwoorden — **Korrelgrens, segregatie energie, DFT, atomaire schaal**

I. Inleiding

Het is vaak verrassend hoe veel invloed legeringselementen kunnen hebben op de eigenschappen van een materiaal, zelfs als ze maar in minieme hoeveelheden aanwezig zijn. Het typevoorbeeld is het ijzer-koolstof systeem. De aanwezigheid van slechts een paar tienden van een procent koolstof is het enige verschil tussen het – althans voor mechanische toepassingen – nutteloos zuiver ijzer en het alomtegenwoordige staal.

De negatieve effecten van onzuiverheden kunnen even indrukwekkend zijn. De aanwezigheid van 45 ppm bismut in koper kan de breekspanning met een factor vier verlagen voor bepaalde tweekristallen[1].

Korrelgrenzen spelen een kritieke rol in dergelijke situaties. In tegenstelling tot andere defecten vormen ze een continu netwerk doorheen polykristallijne materialen en houden ze dus in feite het hele materiaal samen. Bovendien zijn korrelgrenzen kristallografische defecten. Onzuiverheden in de buurt van een defect zijn vaak energetisch bevoordeeld tegenover onzuiverheden in de bulk. Zo is er een drijvende kracht die korrelgrenzen in onzuiverheden verrijkt tot ver boven de gemiddelde bulkconcentratie. Dit is de segregatie energie.

De segregatie energie hangt af van de exacte atoomconfiguratie in de korrelgrens.[2] Helaas is dit verband buiten het bereik van het experiment. Beide aspecten van het probleem zijn immers problematisch: het meten van de segregatie energie en het bepalen van de exacte atoomconfiguratie aan de korrelgrens.

Alternatieven voor het experiment zijn dus nodig. Ab initio berekeningen bieden zo een alternatief. Vertrekkende van de gevestigde wetten van de fysica, inclusief de postulaten van de kwantummechanica, is het in principe mogelijk om elk systeem op een atomaire schaal te beschrijven, exact die schaal die relevant is voor korrelgrenssegregatie. Voor dit werk is Density Functional Theory (DFT) gebruikt.

II. Het gemodelleerd systeem

DFT past doorgaans periodieke randcondities toe als het om vaste materie gaat. Dit limiteert de mogelijke korrelgrenzen, aangezien deze een kleine herhalingscel moeten hebben. De meeste grenzen hebben niet zo een kleine cel, ze worden daarom vaak willekeurig genoemd.

Om een model te kiezen dat de realistische willekeurige korrelgrenzen zo goed mogelijk benadert wordt naar de korrelgrensenergie gekeken. Hierbij is verondersteld dat korrelgrenzen met een gelijkaardige energie gelijkaardige eigenschappen hebben. Willekeurige korrelgrenzen hebben doorgaans een hogere energie dan de speciale korrelgrenzen die met DFT gemodelleerd kunnen worden. Een speciale korrelgrens met toch een redelijk hoge energie is de aangepaste $(2\bar{2}1)$ Σ9 [110]. Toch is de energie laag genoeg zodat de korrelgrens nog voorkomt.[3] De grens is aangepast omdat de standaard Σ9 korrelgrens twee atomen bevat die zeer dicht bijeen komen, als getoond in Figuur 1, wat geen realistische situatie is.

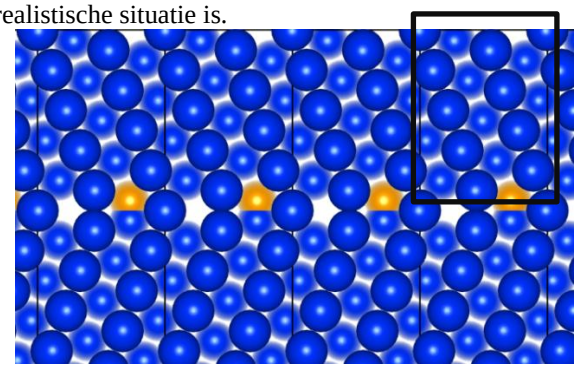

Figuur 1: Een zicht langs de [110] as van de Σ9 grens. De zwarte lijnen duiden de herhalingscellen aan. De wazige atomen bevinden zich in een ander blad dan de pagina. In de aangepaste grens zijn de gele atomen verwijderd. De zwarte kader geeft de positie van Figuur 2 aan.

DFT kan ook maar een beperkt aantal atomen modelleren, een eenheidscel met honderd atomen is al een groot systeem. Bijgevolg kan de laagste concentratie voor een onzuiverheid minimaal 1 at% zijn. Om problemen met oververzadiging te vermijden werd gewerkt met fosfor, wat een redelijke oplosbaarheid heeft in koper.

III. Resultaten

A. *Validatie van het modelsysteem*

Twee tussenresultaten zijn belangrijk om de kwaliteit van de berekeningen te controleren.

De berekende korrelgrensenergie voor de aangepaste $(2\ \bar{2}\ 1)$ $\Sigma 9$ [110] is 837 mJ/m². Deze waarde is ~10% groter dan typische experimentele waarden en toont een goede overeenkomst met andere ab initio berekeningen op speciale korrelgrenzen.[4, 5].

Aangezien de grootte van de herhalingscel in DFT beperkt is, is het ook interessant om te controleren hoe veel invloed de aanwezigheid van een korrelgrens in de cel heeft. Dit kan gedaan worden door de valentie-elektronendichtheid te vergelijken voor een cel met en een cel zonder korrelgrens. In Figuur 2 zijn de niveauoppervlakken van dit verschil getoond in een eenheidscel.

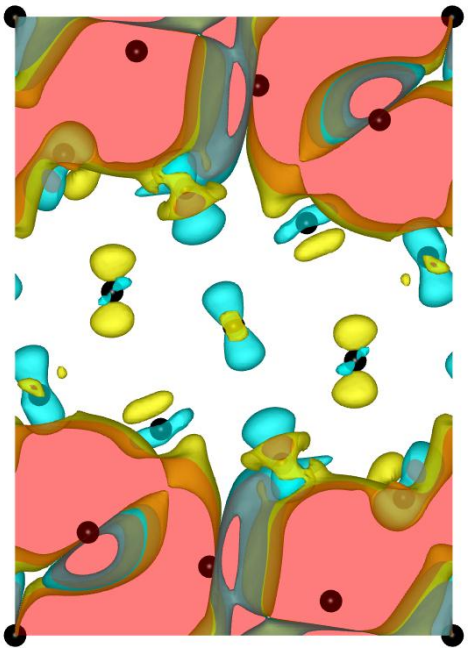

Figuur 2: Niveauoppervlakken voor ± 10^{-3} elektronen per nm^3. De rode gebieden zijn doorsneden van de niveauoppervlakken met het zichtvlak, de zwarte sferen stellen de atoomposities voor. De korrelgrenzen zitten aan de boven- en onderkant van de figuur.

Alhoewel de invloed van de korrelgrens duidelijk doorheen de hele cel gevoeld wordt, is er toch een relatief groot gebied waar het verschil in elektronendichtheid minder dan 10^{-3} elektronen per nm^3 is. Te vergelijking: de gemiddelde dichteheid van de valentie-elektronen is 864 en 915 elektronen per nm^3 voor de korrelgrens en de bulk respectievelijk. Deze is echter wel sterk gelokaliseerd rond de kernen.

Dat de cel met de korrelgrens toch een gebied bevat waar de omgeving op die van bulk koper lijkt, wordt geïndiceerd door de vergelijking gemaakt in Tabel 1.

Tabel 3: Energiekost om een vrij fosforatoom in bulk koper te brengen en een gebonden koper atoom naar een vrij atoom te herleiden

Bulkachtig	-1.256 eV/atoom
Echte bulk	-1.241 eV/atoom

Het verschil is 0,015 eV/atoom of 1450 J/mol. Ter vergelijking, een lage segregatie energie is typisch meer dan 40 kJ/mol, zo een 0,4 eV/atoom[5].

B. *Segregatie energie*

De segregatie energie werd berekend voor vier substitutionele posities op de korrelgrens en één interstitiële positie. De resultaten in Tabel 2 hebben de conventie dat een negatieve segregatie energie impliceert dat een positie op de korrelgrens voordeliger is dan in de bulk.

Tabel 4: Segregatie energieën voor verschillende posities op de korrelgrens.

Subst. 1	-0.588 eV/atoom
Subst. 2	-0.466 eV/atoom
Subst. 3	+0.049 eV/atoom
Subst. 4	-0.175 eV/atoom
Interstitieel	+0.348 eV/atoom

Twee van deze waarden zijn typische segregatie energieën zoals hiervoor vermeld. De andere plaatsen zullen niet of weinig bijdragen tot de segregatie. De holte blijkt te klein te zijn voor het fosforatoom. Opmerkelijk is dat positie 1 en 2 dichtere koperburen hebben dan positie 3 en 4.

Na relaxatie streven de fosforatomen naar een kortere afstand met koperburen dit gebeurde simultaan voor alle buren. Met andere woorden, het verkorten van de fosfor-koper afstanden gaat ten koste van de koper-koper afstanden..

IV. Nauwkeurigheidsstudie

Misschien zelfs belangrijker dan het resultaat zelf is een schatting van de onzekerheid van het resultaat. Afwijkingen komen van twee kanten: de numerieke fouten uit de berekeningen zelf en de intrinsieke fouten aan het gekozen model

A. *Onzekerheid over de berekeningen*

De uiteindelijke segregatie energie is het verschil tussen de energie van een cel met een fosfor atoom in de bulkachtige omgeving en van een cel met een fosfor atoom op de korrelgrens. Alhoewel veel

verschillende factoren de fouten op de berekeningen veroorzaken, bleek dat één bron domineerde. Wanneer het aantal termen in de reeks van vlakke golven die gebruikt worden om de elektronendichtheid te benaderen toenam, dan schommelt de elektronendichtheid. Bij de gebruikte reeksgrootte bleek deze schommeling nog 10 meV te bedragen, wat vier keer groter is dan andere numerieke foutbronnen.

B. Fouten op het model en methode

Twee mogelijke bronnen van fouten op het model werden reeds aangehaald in sectie III.A: het verschil tussen een willekeurige korrelgrens en de gewijzigde Σ9 korrelgrens en het verschil tussen de bulkachtige omgeving en een echte bulk omgeving.

Bijkomende fouten worden veroorzaakt door de periodiciteit van het systeem. De onzuiverheden en vooral de korrelgrenzen worden zeer dichtbij herhaald en deze kopieën zullen elkaar dus beïnvloeden. Ook wordt de segregatie energie berekend voor een discrete sprong in concentratie: ofwel bevat de korrelgrens een atoom ofwel niet, terwijl de echte segregatie energie zou moeten afhangen van een infinitesimaal concentratieverschil. Ten slotte is de DFT methode per definitie niet exact, anders zouden berekeningen onmogelijk zijn.

Het inschatten van de grootte van deze fouten is moeilijk. Eigenlijk kan alleen vergelijking met het experiment gebruikt worden om de fout door de DFT benaderingen in te schatten. De fout van 0,015 eV in Tabel 1 is een indicatie dat de fout door de periodiciteit van de korrelgrens beperkt is. Sinds fosfor een redelijke oplosbaarheid heeft in koper wordt ook verondersteld dat de interacties tussen de herhaalde fosforatomen beperkt zullen zijn.

V. CONCLUSIE

De segregatie energie is berekend voor fosfor in een koper Σ9 korrelgrens. Het resultaat ligt binnen de verwachtingen en is geschat op een factor tien groter dan de fouten door berekeningen en modelkeuze. Er werd ook een verband waargenomen tussen de afstand tussen de dichtste buren en de segregatie energie voor die positie. Ten slotte werd ook nog de vaststelling gedaan dat de fosforatomen bij relaxatie al hun bindingen verkorten, en dus niet een paar opofferen ten voordele van anderen.

Door het inzicht verkregen door deze berekeningen is de gevolgde methode succesvol te noemen en kan ze dus in de toekomst herhaald worden voor gelijkaardige berekeningen.

DANKWOORD

Dit werk werd uitgevoerd met de Stevin Supercomputer Infrastructuur bij Universiteit Gent, gefinancierd door de Herculesstichting en de Vlaamse overheid, departement EWI. De kristallografische van de Crystallographic Open Database[6] werd gebruikt om de cellen te maken. De auteur zou ook graag de medewerkers van het Centrum voor Moleculaire Modellering bedanken voor hun advies en steun.

REFERENTIES

[1] Li, G.H. and L.D. Zhang, R*elationship between misorientation and bismuth induced embrittlement of 001 tilt boundary in copper bicrystal.* Scripta Metallurgica Et Materialia, 1995. **32**(9): p. 1335-1340.

[2] Alber, U., H. Mullejans, and M. Ruhle, *Bismuth segregation at copper grain boundaries.* Acta Materialia, 1999. **47**(15-16): p. 4047-4060.

[3] Ikeda, K.-i., et al., *Grain boundary structure of ultrafine grained pure copper fabricated by accumulative roll bonding.* Materials Transactions, 2008. **49**(1): p. 24-30.

[4] Hu, J.R., et al., *HRTEM investigation of the multiplicity of Sigma=9 01-1 /(122) symmetric tilt grain boundary in Cu.* Materials Chemistry and Physics, 2002. **74**(3): p. 313-319.

[5] Lozovoi, A.Y., A.T. Paxton, and M.W. Finnis, *Structural and chemical embrittlement of grain boundaries by impurities: A general theory and first-principles calculations for copper*. Physical Review B, 2006. **74**(15).

[6] Grazulis, S., et al., *Crystallography Open Database (COD): an open-access collection of crystal structures and platform for world-wide collaboration.* Nucleic Acids Research, 2012. **40**(D1): p. D420-D427.

Table of contents

List of symbols and abbreviations

ppm	Parts per million
DFT	Density Functional Theory
eV	Electron Volt
meV	10^{-3} electron volt
X_b	Fraction of boundary sites occupied
ΔG	Segregation energy
X_c	Fraction of bulk sites occupied
R	Gas constant
T	Temperature
Ψ	Wavefunction of both nuclei and electrons
ψ	Decoupled wavefunction, only
φ	Kohn-Sham orbital
χ	Basis function
ρ	Electron density
$\hat{H}$	Hamiltonian
$\hat{T}$	Kinetic energy operator
$\hat{V}$	Potential energy operator
V	External potential
V_H	Static Coulomb potential
LDA	Local Density Approximation
GGA	Generalized Gradient Approximation
PBE	Functional by Perdew Burke Ernzerhof
LAPW	Linearized Augmented Plane Wave
VASP	Vienna Ab-initio Simulation Package
MPI	Message Passing Interface
GB	Grain boundary or gigabyte
MB	Megabyte
CSL	Coincident Site Lattice
Σ	Reciprocal CSL density
Å	Ångström

1. Introduction

Humans have utilized and produced metals for thousands of years. Despite this long history, metallurgy is still an important field in materials science. The search for stronger, tougher and otherwise more desirable metals is almost as old as the use of metals themselves and is more active than ever. One of the possible routes to improve materials is by adding certain elements. The addition of carbon to iron is a textbook example. Other elements can have equally impressive but adverse effects on the properties of metals. A well-known example is sulfur in steel. Although modern metallurgic processes allow for concentrations of unwanted impurities in the order of tens of parts per million, there is a drive to lower these levels even further.

How can it be that such minute concentrations can have noticeable effects? After all it is our experience in daily life that a concentration of one in one hundred thousand is generally negligible, yet the presence of a mere 45 ppm bismuth in copper can lower the stress needed for fracture by more than a factor of five for certain bicrystals.[1] To understand where these effects come from, one must realize that impurities are generally not uniformly distributed in the material. Locally, concentrations can be orders of magnitude higher than the average. This way, the presence of only minute quantities of impurities can greatly alter the properties of a material.

A grain boundary is one of the places in a material that typically contain higher levels of impurities than the rest of the material. Most crystalline solids, such as metals, are polycrystalline: they consist of many microscopic crystals, called crystallites or grains. If the material undergoes a phase transformation, many grains are usually nucleated simultaneously and grow until they impinge on each other. As grains often nucleate independently, they have different orientations and thus a clear boundary remains. This boundary is called a grain boundary. Places in a material that are relatively far removed from a grain boundary and are not influenced by it are called bulk material.

Grain boundaries are critical locations because they form a continuous network throughout the material. The situation is often likened to that of mortar in a brick wall: if the mortar fails for any reason, the whole wall fill fail, regardless of the quality of the bricks. So if the presence of impurities in the grain boundary makes it easier to mechanically separate the grains, the whole material can fail.

The reason why grain boundaries tend to be enriched in impurities is well understood. The energy of most impurities is lower at a grain boundary and thus the impurities tend to move towards the boundary. The resulting enrichment is called grain boundary segregation. What is not well-known however, is the exact nature of this driving energy difference, the segregation energy. The segregation energy depends on the atomic configuration of the grain boundary and on the impurity. However, such exact configurations are very difficult to determine experimentally. Additionally, the magnitude of the segregation energy can only be determined

indirectly, by comparing the concentration in bulk to the concentration in the boundary.

To gain insight into the effects on an atomic scale, such as the preferred positions of impurities near a grain boundary and the segregation energy on an atomic scale, we turn to ab-initio methods, specifically density functional theory, or DFT. Ab-initio methods rely on the theories of quantum mechanics and not on fitting to experimental values. As such, they offer an independent view and can reinforce experimental knowledge, or as is the case here, provide insight where experimentation is impossible or infeasible.

The goal of this work is twofold. First, the aim is to perform accurate calculations of the segregation energy of phosphorus in a copper grain boundary. This must be seen as a 'pave-the-road' kind of calculation though. The second goal of this work is ensuring reusability. Subsequent efforts on similar problems should be able to reuse as much as possible of the protocols and tools developed during this work

This second goal is typical for computer simulation. Due to the nature of DFT calculations, it only requires a change of parameters to change from one material to another or from one kind of grain boundary to another. Therefore, once the simulations for copper are set-up and properly documented, it is possible to repeat them for any other material, boundary or impurity for only a fraction of human effort. Only the computational expense has to be paid in full for every calculation.

2. Grain-boundary segregation

To fully explain grain-boundary segregation some basic concepts from materials science need to be introduced. In this chapter crystallographic defects will be introduced and the causes, effects and mechanisms of grain boundary segregation will discussed.

2.1. Crystallographic defects

Even a perfectly pure crystal is not perfect: the crystal lattice will always be interrupted somewhere, even if only at the surface of the crystal. Any disruption of the crystal lattice is a crystallographic defect. Defects come in many forms, so they are often classified according to their dimension. The most basic defect, a single missing atom or vacancy, only affects a very small volume around it, and is therefore given dimension zero. As an illustration, Figure 1 shows a model of a vacancy in a [100][1] layer of simple cubic lattice. Note that the layers above and below the plane of this page are completely filled. The result is that the crystal lattice is virtually undisturbed except at the vacancy site. These vacancies are the only defects that are present in appreciable quantities at room temperature in thermal equilibrium.[2] Another example of a defect with dimension zero would be an additional atom, placed somewhere between the other atoms in the lattice, a self-interstitial.

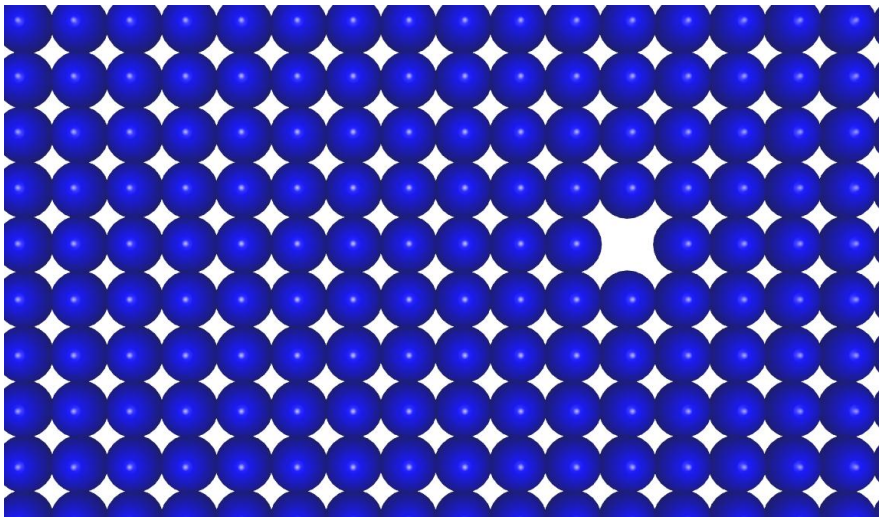

Figure 1: A single vacancy

Defects with dimension one are line-defects or dislocations. In principle they can distort the lattice for an unlimited distance in one direction, but they are very limited in other directions, akin to a one-dimensional curve in three-dimensional space. An example would be an edge dislocation. Edge dislocations can be formed by insertion of a half plane of atoms in a lattice. Only at the edge of the half plane is the lattice distorted. The movement, creation and destruction of dislocations are closely intertwined with plastic deformation and subsequently

[1] It is assumed the reader is familiar with Miller indices. If this is not the case, a book such as [3] can be used as reference work.

with the mechanical properties of a material[4]. Apart from that, their distortion of the lattice can also other properties such as thermal conductivity. As such, they are of great importance for physical materials science[5]. Figure *2* shows a schematic representation of an edge dislocation. The upper half of the crystal contains seven columns of atoms, while the bottom half contains only six. The lattice is only distorted where the extra half plane terminates. In this case, the layers above and below the plane of this page are identical to the layer shown.

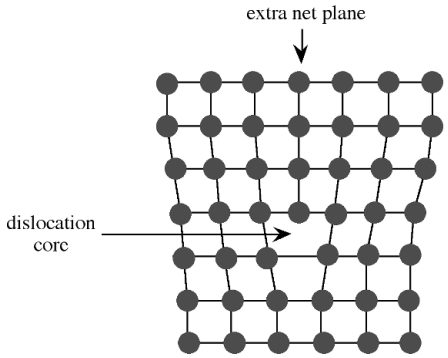

Figure 2: Schematic of an edge dislocation[6]

Although dislocations distort the lattice too much to be present in appreciable quantities at thermal equilibrium, materials generally contain much more dislocations than the equilibrium. Any plastic deformation will cause dislocations to be created. And while, especially at higher temperatures, the number of dislocations in a crystal can be reduced, even a carefully annealed, undeformed sample will contain up to 10^{10} line defects/m² (a surface of 1 m² will be crossed by 10^{10} line defects). A heavily deformed material might contain a hundred thousand times more.[7]

Most materials in practical use are polycrystalline. When the material was formed it underwent a phase transformation, from the melt to solid for example, but this could also be a transformation from one solid into another. Most of these phase transformations happen in a nucleate-and-growth process. The transformation starts with the transformation of a tiny amount of material, called the nucleus[2]. The nucleus of transformed material then grows. In most cases, many nuclei are formed at the same time and after a short growth the newly formed crystallites impinge on each other. Each of these crystallites or grains has a unique orientation of its crystal lattice. While some metallurgical processes aim to create an as narrow distribution as possible, some mismatch is inevitable and thus a clear boundary remains where one grain ended and the next one began. This is the grain boundary. When a polycrystalline material is cut and then carefully prepared, it is possible to distinguish individual grains with the aid of microscopes. Figure 3 shows a scanning electron microscopy image of a ceramic material containing many different grains, The grain boundaries are visible as lines.

[2] Not to be confused with an atomic nucleus.

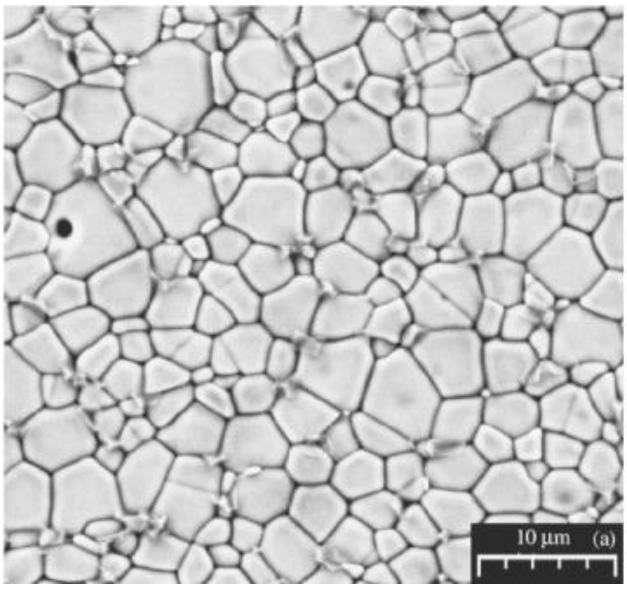

Figure 3: Image of grain boundaries[7]

Grain boundaries two dimensional defects. Most materials contain great amounts of grain boundaries. For example, a material with a relatively coarse grain size with an average diameter of 100 micrometers leads to the order of several hundred square meters of grain boundary for each cubic centimeter of material. Just like dislocations, grain boundaries are of primordial importance for the properties of a material. Not only do they interact with dislocations and directly influence plastic deformation, they have an impact on virtually any material property. As a result, the study of grain boundaries and how to influence them is a major part of metallurgy. What is special about grain boundaries for our purposes is that they form a continuous network throughout the material. Although Figure 3 shows a two-dimensional figure, the grain boundary network is similar to that in a fully three-dimensional material. Important is that grain boundaries will isolate the different grains from each other. Thus, no matter how strong the crystallites themselves are, if the grain boundaries fail for any reason, the whole material will fail.

For completeness, three-dimensional defects should also be mentioned. These are defects such as voids or other phases. They interrupt the lattice over a volume orders of magnitude greater than the defects with dimension zero. While important for macroscopic properties, they are less interesting from an atom-scale point of view, as the crystal lattice is simply absent.

2.2. Interaction with impurities

Apart from crystallographic defects, a crystalline material will also contain impurities. This is unavoidable since the purer a material gets, the harder it becomes to remove impurities. In a crystal lattice, impurities can be present both interstitially, between atoms of the host lattice, and substitutionally, taking the place of a host atom. In both cases the presence of an impurity will distort the lattice around it. This distortion will interact with the distortion created by crystallographic defects. If a defect is close to an impurity, the total energy of the system can

be increased or decreased due to this interaction. In those cases, the defect and the impurity repel or attract each other respectively.

Intuitively, a substitutional impurity that is larger than its host lattice will cause compressive stresses. If it is near a defect that causes tensile stresses, then the energy of the whole system will be lowered compared to the situation where both are far apart. Thus the defect and the impurity attract each other. Even more, a single defect can cause both compressive and tensile stresses in different parts of its immediate environment. It will thus not only attract larger impurities, but also smaller ones. A single defect can be enriched in both small atoms and large atoms. In reality not only size effects, but also electronic interactions play a role[8], it remains true however that many impurities have a lower energy near defects.

The lowering of the total energy when a defect and an impurity are close, so that the respective distortions of the crystal lattice can interact, is a driving force for diffusion. If this diffusion happens against the concentration gradient of the impurity, the defect will become enriched: the impurity segregates to the defect. Hence, the energy difference between an impurity in the bulk and an impurity at a grain boundary is called the segregation energy. In this work the convention is followed that a negative segregation energy means the impurity at the grain boundary is energetically favored.

For grain boundaries this segregation energy is usually negative. As a result, grain boundaries will generally be enriched in whatever impurities that might be present in the material. This enrichment is called grain boundary segregation. The locally increased concentrations at a grain boundary can be orders of magnitude larger than their average concentration throughout the bulk material. To estimate the increase in concentration, the following can be useful.

Assume that there are a fixed number of possible locations for the impurity in the bulk and at the grain boundary. If the energy at the grain boundary is lower, then it is more likely to find a single impurity at a grain boundary site than in a bulk site. The Boltzmann distribution determines how much more likely this is. Assume also that the energy difference between the bulk and the grain boundary remains constant regardless of the presence of other impurities, i.e. the impurities do not interact. It can be shown then that the following relationship holds between the fractional occupancy of the bulk and that of the grain boundary. This is the Langmuir-McLean theory.[9]

$$\frac{X_b}{1-X_b} = \frac{X_c}{1-X_c} e^{\frac{-\Delta G}{RT}}$$

Here, X_b is the fraction of sites occupied at the grain boundary, X_c is the fraction of sites occupied in the bulk material, which can be linked to the concentration, ΔG is the segregation energy and R and T are the gas constant and the absolute temperature respectively. Figure 4 shows a plot of X_b in function of ΔG for two temperatures. The bulk concentration is 1/1000. The red solid curve is for 900 K, the blue slash-dot curve is for 700 K. If the temperature approaches zero, the curve moves towards a discontinuous jump at $\Delta G = 0$.

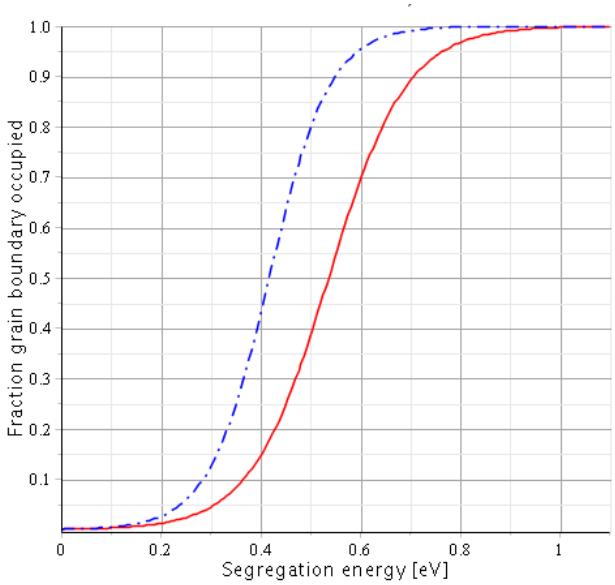

Figure 4: Langmuir-McLean curves

Although this model is far from perfect, as it is unclear how fractional occupancies of possible locations relate to atomic concentrations and it is obvious that, especially at higher concentrations, impurities will interact, this model is nonetheless useful. It implies that even for a low-end segregation energy of 30 kJ/mol, or 0.35 eV/atom, the concentration near the defect can be a hundred times the bulk concentration at 900K.

2.3. Importance of grain boundaries

As mentioned before, grain boundaries are critical defects because they form a continuous network throughout the material, separating the different grains from each other. An important parameter is the strength of the cohesion between two grains that share a grain boundary. An often used metric is the amount of energy needed per unit surface to separate two grains at their grain boundary. This is called the grain boundary cohesive energy for that particular grain boundary, cohesive energy for short. This is not to be confused with the cohesive energy of a material: the energy needed to separate the material in its constituent free atoms. The latter is expressed in units of energy per atom while the grain boundary cohesive energy has units of energy per surface area.

There are two basic modes of fracture in a metal. The fracture can occur because the grains themselves break or because they lose their cohesion. In the first case the fracture is called transgranular, in the second case the fracture is called intergranular. If the increased presence of impurities in the grain boundaries lowers their cohesive energy both modes are affected differently. A metal that normally breaks in an intergranular mode will fail at lower stresses. On the other hand, metals that normally break in a transgranular fashion will at first be virtually unaffected by a reduction in cohesive energy. However, when the cohesive energy is

lowered enough, the mode of fracture will change from transgranular to intergranular.

The lowering of cohesive energy due to grain boundary segregation can be especially dangerous in the following scenario. Imagine a material that normally undergoes quite some deformation before fracture. If impurities are added to the material which undergo grain boundary segregation and lower the cohesive energy, then the material will fracture at lower stresses. If the stress for fracture becomes lower than the stress needed to deform the material, then fracture will occur without prior plastic deformation. This is highly undesirable as there is no visible warning before the material breaks, even though visible deformation is expected for the material in question. This kind of fracture can happen unexpectedly in that case. Combined with the fact that grain boundary segregation is difficult to establish, this can lead to disastrous consequences.

There are several mechanisms that explain the effects that impurities have on the grain boundary cohesive energy. Again one can intuitively grasp the size effect: the presence of differently sized atoms distorts the lattice and can push the two sides of a grain boundary apart. The presence of impurities also has an influence on the local distribution of electrons. Impurities in a grain boundary can form strong, covalent-like bonds.[10] These bonds influence the metallic binding of the host atoms across the grain boundary. As a result the cohesive energy can either decrease or increase.[11]

Apart from acting on the cohesion energy, grain boundary segregation influences a whole range of other properties. Generally, any mechanism that acts specifically on grain boundaries will be influenced by grain boundary segregation. An example is creep: materials under constant stress will slowly deform, especially at higher temperatures. One of the mechanisms of creep is diffusion of atoms along grain boundaries. Logically, grain boundary segregation influences creep, sometimes in unexpected ways. A high concentration of impurities in a grain boundary might increase the formation of voids during creep[12] and thus greatly hasten failure. However, sometimes creep is slowed by the presence of impurities in grain boundaries. In such cases grain boundary segregation would be desirable. Finding elements that slow creep is an active area of research.[13]

The chemical composition of a material also has a great influence on its corrosion properties. Due to grain boundary segregation, the composition at a grain boundary can be markedly different from the one in bulk. As such, grain boundaries might corrode much faster than the bulk material. This can lead to intergranular corrosion, a mode of corrosion concentrated on the grain boundaries. Since the grain boundaries form a network throughout the material, failure can occur when only a small fraction of the total material has corroded. Similarly, stress corrosion cracking can be influenced. Stress corrosion cracking is the formation and growth of cracks in a corrosive environment under applied stress. If the cracks coincide with grain boundaries, grain boundary segregation will play a role.[14]

2.4. Note on kinetics

It is important to keep in mind that in the discussion above, there is no mention of the kinetics of segregation and only the equilibrium condition is considered. In reality, equilibrium conditions will be never reached. Even more, at room temperature, the diffusion of most impurities is negligible and they are effectively frozen in place. Combined with the fact that the equilibrium shows less segregation with increasing, see Figure 4, this means that the relationship between temperature and segregation is ambiguous. At higher temperatures, segregation will be less pronounced, but will occur faster. Thus the exact history of a material must be known, not only the temperatures at which it was held, but also for how long.

Additionally, equilibrium does not have to be approached monotonously. Non-equilibrium segregation is a well-established effect.[15] This mode of segregation can lead to an overshoot in the concentration at the grain boundary, meaning that the segregation can be worse than predicted by thermal equilibrium. Non-equilibrium segregation is caused by the interaction between impurities and vacancies, a mobile defect of dimension zero which is in fact a single missing atom in the crystal lattice.

Grain boundaries can be sinks or sources of vacancies under stress, deformation or even when the material undergoes a sudden temperature drop. When grain boundaries act as vacancy sinks, vacancies will tend to move towards the grain boundary. However, because vacancies and the impurity atoms prefer to remain close together due to their interacting lattice distortion, some impurity atoms will be dragged along towards the grain boundary. If this mechanism drags more impurity atoms towards the grain boundary than that can diffuse away, then the segregation will be larger than predicted. Of course, if the deformation stops or the stress is taken away, the system will again evolve to the state of thermal equilibrium.

In this work, kinetics will be disregarded. The only variable that will be considered is the segregation energy, a very important quantity to understand equilibrium segregation. As all systems evolve to the state of equilibrium it is felt that this limitation is justified.

2.5. Atomic scale

Although grain boundary segregation is widely known and an important phenomenon in metallurgy, its explanation remains phenomenological. Models exist that predict grain boundary segregation when the driving force is given, but how this driving force depends on the exact atomic configuration in the grain boundary remains unknown. It would be exceedingly difficult to establish such a relationship by performing physical experiments for two reasons.

First there is the problem of simply observing the atomic configuration in the grain boundary. Methods such High-resolution transmission electron microscopy and scanning tunneling microscopy can resolve individual atoms, but these methods only obtain a two dimensional image. This is insufficient to completely describe the configuration of a grain boundary

except in special cases, such as an image of a grain boundary perpendicular to the image plane. On the other hand, methods which allow for the extraction of three-dimensional information from a sample, such as X-ray diffraction, work on scales larger than the thickness of a grain boundary. Thus, merely knowing the atomic configuration at a grain boundary is non-trivial.

Secondly, it is impossible to measure the segregation energy directly. A possible indirect method is observing the evolution of the impurity concentration in function of temperature for several bulk concentrations. From that information is it possible to calculate the segregation energy with a model such as the previously mentioned one of Langmuir and McLean.

However, a deeper insight into the atomic mechanism is not only an advance in fundamental knowledge, it might also lead to practical applications. If it is known which grain boundaries are less sensitive to segregation, it could be attempted to process a material such a way that contains mainly those boundaries.[16] Even if this seems far off, understanding the relationship between atomic configuration and segregation energy could in the very least be used to check and improve existing macroscopic models.

A way to obtain this insight separate from the classical experimentation is the ab-initio approach. Starting from well-established physical principles and the postulates of quantum mechanics, it is possible to calculate the interactions between individual atoms. From there, a system can be constructed simulating a grain boundary. This approach reverses the problem in a way. Rather than discovering the exact atomic configuration and energies from experiment, we give the configuration as a parameter and obtain the corresponding energy relatively accurately. The difficulty is then to make the modeled system resemble reality.

3. The ab-initio method: Density Functional Theory

A basic background in ab-initio methods in general and Density Functional Theory in particular is essential to understand this work and its references to literature. This chapter will provide an overview of Density Functional Theory, or DFT, method. This will be followed by the used software implementation of DFT: the Vienna Ab-initio Simulation Package.

3.1. Ab-initio methods

Ab-initio calculations in their most pure form use no information from any experiment. In other words: they are not fitted to experimental data. Instead, ab-initio methods are based on the laws of physics. As we work on an atomic scale, the postulates of quantum-mechanics are especially important. Central is that these state that everything we can know about a system can be derived from its wavefunction. The wavefunction of a system can be found by solving its Schrödinger equation.

$$\hat{H}\Psi = E\Psi$$

Here, $\hat{H}$ is the Hamiltonian operator, E is the energy of the system and an eigenvalue of Ψ, the wavefunction of the system. Ψ is a function of the coordinates of all particles in the system. The form of the Hamiltonian is known and consists of potential energy V and kinetic energy T terms. The potential is due to the electromagnetic interaction between the particles.

$$\hat{H} = \hat{T} + \hat{V}$$

While this equation can be solved for simple systems, this is not possible for the systems necessary to describe a grain boundary. In order to construct a system even only resembling a grain boundary, it is necessary to include many atoms. A single copper grain easily has a diameter of several micrometers, or a volume in the order of 10^{-15} m³, in the case of copper this corresponds to the order 10^{-14} kg or 10^{11} atoms.

Even if it is not necessary to model such a large system, in order to model the bulk characteristics of a material, it is unlikely that the system could be made smaller than several thousand atoms. For example, a single impurity can have an influence more than ten atoms away,[17] leading to thousand atoms in three dimensions. Even then, the free surface of the crystal would most likely be felt more than a single impurity, meaning that the calculations would be performed on something resembling a nanocrystal rather than bulk material.

A system with thousands of atoms contains tens of thousands of electrons. Each electron has both a three-dimensional position and a spin, totaling four coordinates. As said above, the wavefunction is a function of the coordinates of all particles in the system. A system with tens of thousands of electrons would have four times as many coordinates. A function of a hundred

thousand variables is not only impossible to calculate, but even if it were known, it would be impossible to extract information from it. Thus, for solids at least, the exact Schrödinger equation must be abandoned and instead approximations must be made. These approximations will lead to the DFT method and they will be introduced step-by-step in what follows. For a more thorough treatment of the subject, the reader is referred to any of these references, which were used as a basis for the following sections. [18-20]

3.2. Born-Oppenheimer approximation.

The mass of a nucleus is much larger than that of an electron. In the case of copper, the ratio is more than one hundred thousand. If the momentum of both nuclei and electrons is of the same order of magnitude, the speed of the nuclei would be negligible. As our frame of reference is centered on the center of mass, the net momentum must be zero and we can assume the moment of electrons and nuclei is comparable. Hence, it is acceptable to neglect the kinetic energy of the nuclei and to see them as immobile. This is the Born-Oppenheimer approximation.

With this in mind, the positions of the nuclei become parameters in the wave equation or equivalently: the wave equation for the nuclei becomes decoupled from the wave equation for electrons.

$$\Psi = \psi_e \times \psi_n$$

Where ψ_e is the wavefunction of the electrons only and ψ_n is dependent on the nuclei. For our application of DFT we are mainly concerned with ψ_e and the subscript is dropped. The nuclei are then mainly important because they influence the electrons. We can interpret this as if the nuclei provide a fixed, external potential V which determines the properties of the wavefunction of the electrons.

Although this simplifies the Schrödinger equation to a great extent, while incurring a negligible error for systems with heavy atoms, the resulting equation is still far from solvable and thus further approximations are required.

3.3. First theorem of Hohenberg-Kohn

From the previous paragraph, we know that an external potential, i.e. the location of the nuclei, determines the ground state wavefunction to the Schrödinger equation after the Born-Oppenheimer approximation. It is also very intuitive that this wavefunction relates to exactly one potential, after all it is postulated that all observable properties of the system can be derived from the solution to the Schrödinger equation, including the position of the nuclei and thus the external potential. This means that the wavefunction and the external potential are interchangeable. This derivation is not mathematical rigorous, a more thorough examination would introduce some constants and conditions that would not alter the idea of interchangeability. This is beyond the scope of this work however.

$$V \leftrightarrow \psi$$

Additionally, every wavefunction determines at most one electron density of the system (i.e. the probability to find an electron at that location). Again we come to this conclusion by reasoning that the electron density can be derived from the wavefunction and thus a given wavefunction can not lead to multiple electron densities. What is surprising however, and this is the core of the first theorem of Hohenberg-Kohn, is that every electron density determines at most one wavefunction as well. In other words, the wavefunction ψ and the electron density ρ are also interchangeable.

$$\psi \leftrightarrow \rho$$

Combined, the previous means that the electron density and the external potential are interchangeable. Thus it is possible in principle to determine the electron density from the external potential and vice versa.

$$V \leftrightarrow \psi \leftrightarrow \rho$$

$$V \leftrightarrow \rho$$

As the electron density and the wavefunction are interchangeable, any information obtainable from knowledge of the wavefunction is also obtainable from knowledge of the electron density. In particular, it can be shown that all observable properties of the ground-state system, derived from the wavefunction with an operator O as:

$$\langle \psi | \hat{O} | \psi \rangle$$

can be written as a functional of the electron density ρ.

$$O[\rho]$$

3.4. Method of Kohn-Sham

So far no practical ideas are introduced. It is simply stated that in principle knowledge about the ground state electron density can provide us with knowledge about all observable properties of the system, without having to explicitly know the wave function. Although methods exist to calculate the electron density from the external potential, it is possible to take another approach as well. The method of Kohn-Sham is such an approach and the basis for the DFT method.

One of the reasons why it is impossible to solve the Schrödinger equation exactly for large systems is because the wavefunction depends on so many variables. The method of Kohn-Shan simplifies this problem. An imaginary system is constructed consisting of non-interacting pseudoparticles, rather than the interacting electrons in the real system. Although this system has by definition no physical meaning, it is constructed in such a way that the density of these imaginary particles is the same as the ground state electron density of the real

system. This density is given by:

$$\rho(\vec{r}) = \sum_{i=1}^{N} \varphi_i^*(\vec{r})\varphi_i(\vec{r})$$

Where N is the number of particles in the system, $\vec{r}$ is the spatial coordinate and φ_i is the so-called Kohn-Sham orbital of particle i. The Kohn-Sham orbital serves a similar purpose as the wavefunction.

Knowledge about the electron density of a system is very useful. Because of the Hohenberg-Kohn theorem, it is possible to obtain all information about the real system by knowing its electron density.

The real advantage of the Kohn-Sham method is that the pseudoparticles are non-interacting, meaning that it is no longer necessary to solve a single wave equation for a system containing many particles. Rather, many wave equations must be solved, but each equation only depends on the parameters of one particle. This greatly simplifies calculations, to the point that they are feasible to carry out in practice.

$$\hat{H} = \hat{T} + \hat{V} + \hat{V}_H + \hat{V}_{xc}$$

Here, the Kohn-Sham Hamiltonian is very similar to the one used in the Schrödinger equation after the Born-Oppenheimer simplification. T represents kinetic energy operator and the operator V the potential from the nuclei. To correct for the fact that the pseudoparticles do not interact with each other, two additional terms are included. The most obvious being the Coulomb potential V_H resulting from a static distribution of all the pseudoparticles.

Electrons interact in other ways than by their charge though. So apart from the static Coulomb potential, two more additions are necessary to fully link the Kohn-Sham equations to the real system. First there is a certain interaction of electrons, due to the Pauli exclusion principle. This is called the exchange energy. Second, the kinetic energy and the potential energy of the non-interacting Kohn-Sham pseudoparticles are slightly different from the respective energies of the interacting electrons. This energy difference is called the correlation energy. Exchange and correlation are grouped in the exchange-correlation energy given by V_{xc}. With this extra correction, the density resulting from the Kohn-Sham particles can be made to be equal to the electron density in an interacting system.

Both the static Coulomb potential and the exchange-correlation energy depend on electron density of the system. But this density is calculated from the wavefunctions which are determined by the Kohn-Sham equations. And to write down the Kohn-Sham equations, the static potential and the exchange-correlation must be known. Thus, the Kohn-Sham equations must be solved iteratively starting from a guessed electron density, so that the solution is self-consistent.

3.5. Exchange-correlation functional

It is obvious that the exchange-correlation energy depends on the electron density. If more electrons are packed closer together they will interact differently. Thus a functional must exist that maps a density to its corresponding exchange-correlation energy. This functional is needed to write down the Kohn-Sham equations, but this functional is unknown. On the other hand, and this is one of the strengths of the DFT method, the exchange-correlation is usually relatively modest. So using an approximation for the exchange-correlation energy should give acceptable results.

The exchange-correlation functional is not a complete mystery however. If the electron density is constant in all space, it is possible to accurately calculate the exchange-correlation energy per unit volume with quantum Monte Carlo methods. Such a uniform electron gas is called jellium. In jellium, the negative charge of the electrons is compensated by a homogeneous positive background charge. The number of electrons per unit volume can be taken arbitrary.

A first approach to construct an approximation to the true exchange-correlation functional uses the results for jellium. In the Kohn-Sham equations, space is divided in small blocks. Each block has an average electron density and is assigned the exchange-correlation energy of a block of jellium with the same volume and with the same average electron density. This approach can be expanded to the limit of infinitesimally small cells. This is the Local Density Approximation or LDA.

$$E_{xc}[\rho] = \iiint \varepsilon_{xc}\big(\rho(\vec{r})\big).\rho(\vec{r})\, d^3r$$

Here the exchange-correlation functional E_{xc} is a functional of the electron density. $\varepsilon_{xc}(\rho)$ is the exchange-correlation of jellium with uniform density ρ.

In spite of being a basic approximation, the LDA approach is quite successful. However, it is not perfect and the drive and effort to find better functionals remain. There is no clear method to find improved functionals though. As a result, many functionals are known and used today, each often giving good results for one kind of problems, but worse for others. This leads to the situation where a researcher wishing to describe the bonds in a molecule will use a different functional than one researching bulk materials.

One family of functionals uses the generalized-gradient approximation or GGA. Basically, these functionals try to improve the LDA by not only taking the local electron density into account, but also the local gradient of the density. One of the most popular GGAs for crystals and the one used in this work is the one introduced by Perdew, Burke and Ernzerhof, the so-called PBE-functional.[21]

3.6. Numerical solution

The way in which the Kohn-Sham equations are solved numerically is by expressing the Kohn-Sham orbitals into a known basis.

$$\varphi_i(\vec{r}) = \sum_{a=1}^{\infty} c_a^i \chi_a^i(\vec{r})$$

φ_i is again the Kohn-Sham orbital of particle i, $\vec{r}$ the spatial coordinate, c^i is a series of constants and χ^i are the basis functions.

In reality it is impossible to work with an infinite sum, so this series will be cut. The point at which this cut-off happens is one of the parameters that must be chosen for calculations. A higher cut-off will mean a better approximation, at the expense of more memory requirements and longer calculations times.

Again several basis sets are known, each particularly suited for different applications. Sets that converge rapidly are called soft and they can tolerate fewer terms in the expansion. However, it might take more computational effort to work with these sets. Another property of sets is their transferability. Some sets only give good results for a certain type of problem, others are more broadly applicable. Therefore the selection of the basis sets is an important decision. In this work Projector Augmented Waves are used as a basis, see also the paragraph in section 3.8. on the Projector Augmented Waves.

The Kohn-Sham orbitals are then determined by the coefficients of their basis functions. As the Hamiltonian is linear, this means that that the Kohn-Sham equations can be put into matrix form. This matrix formulation is then solved using algorithms from linear algebra. In particular, a version of a block Davidson method was used, an iterative procedure.

$$HC = SCE$$

Here H is a matrix containing the results of the Hamiltonian working on the basis functions. E are the eigenvalues of the system. S is an overlap matrix, it is a diagonal matrix if the basis functions are orthonormal. C are the unknown coefficients.

3.7. Periodic boundary conditions

The method under consideration now is already a great simplification from the original Schrödinger equation. However, it is still out of reach of current computational power to examine systems with the desired amount of particles. In the previous example of a single grain, anywhere up to 10^{10} atoms should be included.

Introduction of periodic boundary conditions brings calculations on bulk materials within reach. Only the description of a small unit is necessary, and this unit is repeated infinitely in space. This unit is very small for most crystals, containing only a handful of atoms, and is

thus easily described. A disadvantage of periodic boundary conditions is that if the repeating unit contains a crystallographic defect or impurity, this is also repeated. Since we are usually interested in the properties of only a single defect, care must be taken to prevent the repeated defects from influencing each other. A basic method to achieve this is making the repeating cell larger and including more atoms, so the defects are repeated further from each other in space. This way the advantage of the very small repeating cells is lost, but the resulting systems are still much smaller than what would be needed to describe a complete crystal without periodic boundary conditions.

The figures below illustrate how a larger repeat cell can be used to modify the environment of each defect. Both figures are views along [100] of a body-centered cubic lattice. The brown atoms are the host atoms and the smaller, purple atoms are impurities. Fuzzy atoms lie half a lattice parameter below the plane of this page. The repeat units are bounded by the black lines. In Figure 5, the repeat unit contains only two atoms, while this means it is easy to describe the system, this also implies half the atoms in the system will be impurities. Figure 6 shows a repeat cell twice as large in each dimension. As a result it contains 16 atoms, of which 8 are visible. Only one in 16 atoms is an impurity at the cost of longer computation times and more memory requirements for solving that system's equations.

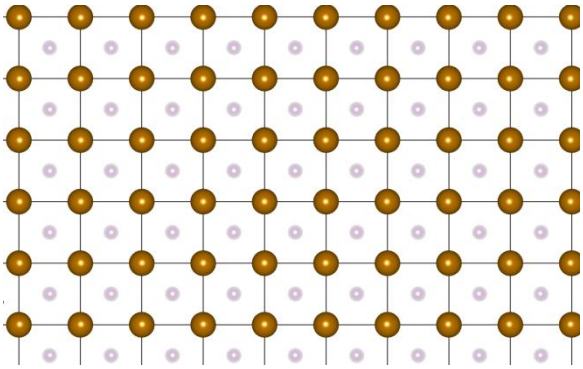

Figure 5: Impurities in small repeat unit

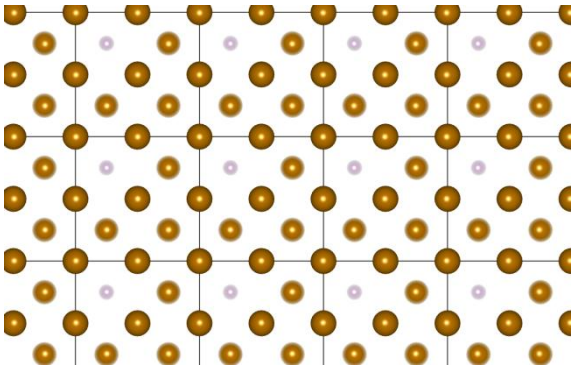

Figure 6: Impurities in larger repeat unit

Additionally, a periodic system implies a periodic electron density. The periodic nature of plane waves makes them particularly suited as basis functions for the Kohn-Sham equations. Plane waves are also easy to work with due to the fact that their Fourier transforms are simple.

3.8. Core oscillations

A disadvantage of plane waves is that Kohn-Sham orbitals have steep gradients near atomic nuclei and that this behavior is poorly modeled by plane waves. It would require an exceedingly large amount of basis functions to properly describe the orbitals near the nuclei, with the known implications on computational requirements. Several approaches exist to solve this problem.

3.8.1. Pseudopotential

First, a pseudopotential can be used. The purpose of pseudopotentials is to result in a smooth wavefunction near the nucleus, one that can easily be approximated with plane waves. To do this the real potential within a sphere around the nuclei is replaced by a pseudopotential. Outside the sphere, in the interstitial region, the potential is left unchanged. The pseudopotential is chosen so that it results in a smooth wavefunction for that particular atom, while confirming to certain boundary conditions at the edge of the sphere such as scattering behavior. A pseudopotential has to be calculated once for an atomic species, and can then be used for all further calculations involving that atom. An illustration of what a pseudopotential does is given in Figure 7. The blue dashed lines correspond with the potential caused by the presence of the nucleus and the resulting wavefunction. The solid red lines show how an altered potential can smooth the wavefunction. Beyond a certain radius r_c from the nucleus the potentials and wavefunctions are identical.

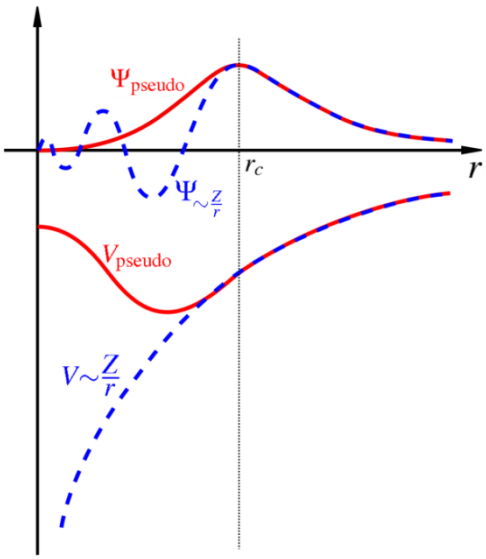

Figure 7: Schematic representation of a pseudopotential.[22]

3.8.2. Linearized Augmented Plane Wave method

Second, the plane waves themselves can be modified. This is the augmented plane wave method and is used in the Linearized Augmented Plane Wave or LAPW method. Just like the pseudopotential method, space is divided in areas near the nucleus, where the Kohn-Sham orbitals oscillate rapidly, and in an interstitial area, where they are smooth. For the smooth orbitals, regular plane waves are used. In the areas close to the nuclei, functions are used that are particularly well-suited to converge to the rapid oscillating orbitals. The coupling between the smooth and oscillating areas relies on several boundary conditions. An advantage is that the behavior in the interstitial space depends little on the nature of the atoms. The dependence is contained in the spheres around the nuclei.

3.8.3. Projector Augmented Wave method

A last method is the Projector Augmented Wave or PAW method.[23] Here, a linear transformation is introduced that transforms the sought Kohn-Sham orbitals. A certain radius

away from the nuclei, the transformed orbitals remain identical. In a sphere near the core, the oscillating orbitals are transformed into a smooth function. The method is more general than the augmented wave method, although the transformation must still be chosen specifically for each atomic species. As the transformation is linear, it can be decomposed in projector functions, hence the name of the method. The PAW method will be used for the calculations in this work.

3.9. Frozen core electrons

A last important simplification is often made by assuming that the electrons near the nucleus are unaffected by the environment of the atom and have no influence on its binding properties. That this assumption is quite reasonable is shown in Figure 8. The electron density for a platinum atom is shown as a function from the nucleus for each electron shell. Only a few shells have noticeable densities beyond a certain radius $r_{c,}$ these are the valence electrons.[23] The wavefunctions for the core electrons are therefore adequately described by the corresponding wavefunctions in the free atom and subsequently do not have to be included in the DFT calculations. The electrons are said to be frozen in place, and an ionic core, rather than a nucleus is used.

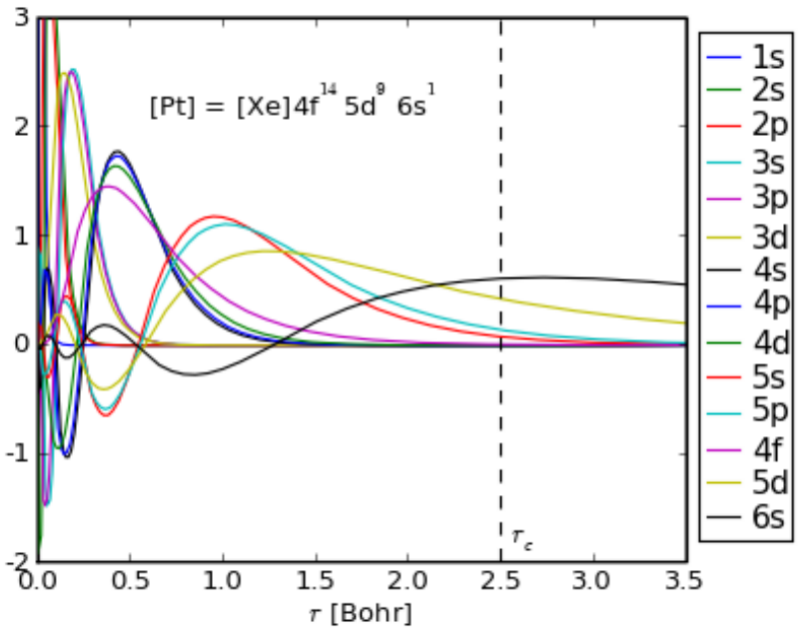

Figure 8: Distance limits of core electrons

Frozen core electrons can readily be combined with the previously mentioned methods to solve the core oscillations, as all information on the core electrons is contained within the sphere around the nuclei. As a result they do not influence the interstitial region.

3.10. Vienna Ab initio Simulation Package

The software used for the calculations in this work is the Vienna Ab initio Simulation Package, or VASP[24]. It is a computer program, capable of performing DFT calculations. It needs four input files, which are described below, to perform DFT calculations on the specified system. Calculated values that were used for this work include the total energy of the system, the pressure acting on the system and its electron density.

VASP is a versatile program: it can also be used to perform calculations other than DFT. Consequently many variables can be specified. Most of the required parameters have sensible defaults, allowing users with incomplete knowledge of the inner workings of the software to work with it. The parameters where the default was not used and those where extra care should be taken are listed below. For a more thorough listing of the capabilities and parameters of VASP, the reader is referred to the VASP manual.[25]

3.11. Files needed for VASP

3.11.1. POSCAR file

As described previously, DFT generally uses periodic boundary conditions for solids and VASP is no exception. With the description of a relatively modest unit that is infinitely repeated, the properties of large systems can be calculated. This repeat unit is called a unit cell. In VASP, unit cells are defined in the POSCAR file. This file contains the Cartesian coordinates of the three unit cell axes and the positions of the atoms inside the unit cell. The position of the atoms can be expressed in Cartesian coordinates or relative to the axes of the unit cell.

Apart from these parameters, the POSCAR file also determines relaxation. Relaxation is the process of moving atoms to minimalize the total energy of the system. It is done by moving atoms according to the forces acting on them. It is possible to specify in the POSCAR file which atoms are allowed to relax and in which directions. This is called Selective Dynamics and was extensively used for the relaxation procedure described in section 4.6.

3.11.2. KPOINTS file

Since the system and the used wavefunctions are periodic, it is convenient to work with their Fourier transformations rather than with their representations in real (or direct) space. The vector space containing the Fourier transforms of direct space is called reciprocal or k-space. Reciprocal space is closely related to direct space. If the configuration in direct space contains shows cubic lattice symmetry for example, then reciprocal space will also have cubic symmetry. Due to the Bloch theorem, all information about the periodic system is contained in the Brillouin zone. The Brillouin zone is a smallest unit cell of reciprocal space. The evaluation of integrals over the whole system can therefore be reduced to evaluations of the Brillouin zone.

However, since computers are discrete, continuous evaluation of the Brillouin zone is not possible. Therefore, all integrals in this zone are only evaluated in a series of points, the so-called k-points. The density of the k-point grid is a critical parameter to obtain good results. A too sparse grid will give incorrect calculations, but calculation time scales exponentially with an increasing number of k-points.

The KPOINTS file determines how many k-points are used and where they are placed. In this work the grids are generated using the Monkhorst-Pack scheme.[26] This scheme divides each axis in the Brillouin zone by a specified integer. Every linear combination of these new, smaller axes determines the location of a k-point. Ideally, the k-point grid is equidistant. However, the axes of the Brillouin zone of the used cells have non-integer ratios, so an exactly equidistant grid is unattainable. The best approximation was used for calculations.

The origin of reciprocal space, the Γ point, is an important point and its inclusion can hasten or slow convergence. However, if the k-point mesh is dense enough, inclusion or exclusion of the Γ point should have a negligible influence. All grids used in this work included the Γ point.

If the system is symmetric, the number of k-points can be reduced by applying symmetry. Only those k-points that lie in the irreducible part of the Brillouin zone need to be evaluated. Other k-points can be mapped to these irreducible k-points by a finite number of rotations and reflections that also preserve the symmetry of the reciprocal space. The irreducible k-points are then weighted in the integrals by the number of k-points they represent.

The absolute density of the grid is determined by convergence tests, performed in section 5.1. A convergence test consists of identical calculations with systematically denser k-point grids. The optimal k-point density is then the lowest density for which a further increase in k-point density does not affect the result of the calculation anymore.

3.11.3. POTCAR file

The POTCAR file contains the pseudopotential or the description of the projectors for the PAW method. These files are calculated in advance for each atomic species and are made available together with the VASP license. For systems with multiple species, POTCARS should be concatenated. Note that each pseudopotential or projector description is made for a certain exchange-correlation functional and the chosen POTCAR should match the used functional.

3.11.4. INCAR file

All parameters not specified in the previous files are provided in the INCAR file. The INCAR file is a text file where parameters are specified in the format "tag=value". If the tag of a certain parameter is not stated in the INCAR file, the default value is used for that parameter. Therefore it is impossible to forget to specify a parameter.

3.12. Important parameters

3.12.1. GGA tag

This tag determines the used exchange-correlation functional. If the value of this tag is unspecified, the functional will default to the one matching the POTCAR file.

3.12.2. ISMEAR and SIGMA tag

In metals the electron occupancy at the Fermi level is discontinuous as the calculations happen at 0 K. Such a sharp drop gives problems: the Fourier transformation of a discontinuous function retains large oscillations, which only get pushed closer to the discontinuity with increasing terms in the expansion. In two dimensions, this is known as the Gibbs effect and is illustrated below. The wild variations at the shoulders can be pressed closer to the discontinuity, but can not be fully eliminated by increasing the number of basis functions by a finite amount, such as is done when going from Figure 10 to Figure 9.

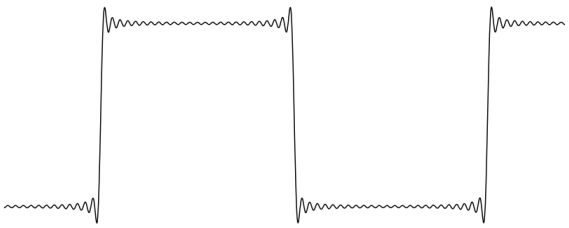

Figure 10: Fourier series approximation with fewer terms[27]

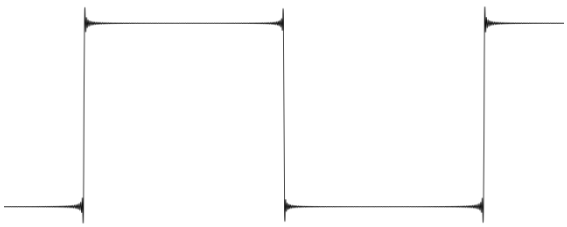

Figure 9: Fourier series approximation with more terms[27]

In order to prevent the discontinuous drop, a smearing method is used. The default is the method of Methfessel-Paxton of the first order. This value is recommended for calculations that include relaxations. The default smearing parameter (SIGMA-tag) is used. If no relaxations are included, then it is recommended to use the tetrahedron method with Blöchl's corrections. These recommendations are followed in this work.

For insulators and semiconductors smearing becomes much less critical, as there is no discontinuity inside a band.

3.12.3. EDIFF tag

This tag determines the convergence limit for the iterations of the electronic structure in the system. This limit is taken at 10^{-5} electron volt. The default convergence limit for ionic updates has a default of 10 times this value. The default for ionic updates was unchanged during calculations.

3.12.4. IBRION tag

This tag determines which algorithm is used to relax ions. The relevant choices are a quasi-

Newton algorithm and a conjugate gradient algorithm. According to the VASP manual, the quasi-Newton method is faster near the optima, while the conjugate gradient method is recommended for worse guesses. As the relaxation of a grain boundary moves some atoms quite far, the conjugate gradient is used for all relaxations.

3.12.5. NSW tag

The maximum number of iterations to relax the ions is given with this tag. As ionic updates were always carried out until convergence, only the value zero was relevant in cases where ionic movement had to be prevented.

3.12.6. LREAL tag

The projector functions in which the transformation of the Plane Augmented Wave method has been decomposed can be evaluated in direct space or in reciprocal space. The advantage of direct space is that the required number of operations remains constant with increasing cut-off of the basis set. In reciprocal space the required amount of operations increases linearly with increasing basis size.

However, working in real space has its problems. According to the VASP manual, there is interference between the high frequency components of the projector functions and the low frequency components of the basis functions, and noise is introduced. To prevent this, the high frequency components of the projectors must be removed. VASP supports several schemes to do this, with one being recommended for general use.

Because of the increase in speed, the projector functions were evaluated in real space and the recommended correction algorithm was used. In the case of final calculations (grain boundary energy, segregation energy, etc.) the increase in accuracy was deemed to more valuable than shorter calculation times and the projectors were evaluated in reciprocal space.

3.12.7. ISIF tag

The ISIF-tag determines two things. First of all it determines whether the stress tensor is calculated accurately. This calculation is somewhat expensive so it was disabled when the stress tensor was not needed. Secondly it determines which parameters are allowed to relax: atomic position, shape of the cell, volume of the cell or combinations. Only atomic positions were ever allowed to relax, optimizations of cell parameters were performed manually.

3.12.8. PREC tag

This tag determines the cut-off of the basis set, the density of the Fast Fourier Transform (FFT) grid and the accuracy of the correction if the projector functions are evaluated in real space. As the optimal cut-off of the basis functions was calculated manually and specified separately, see section 5.2. this tag had no bearing on it. The tag was always set to high, to increase the density of the FFT grid.

3.12.9. Parallelization parameters

The VASP code was run using the High Performance Computer (HPC) infrastructure of Ghent University, called Stevin. This infrastructure consists of several clusters. A cluster itself is a group of connected CPUs, similar to the ones found in a desktop computer for private use. Although in the HPC infrastructure the CPUs are grouped in nodes, within a node resources such as memory are shared. Communication between nodes is much slower than communication within a node. The cluster that was most used for this work, "Gengar", contains more than 150 nodes, each having 16 gigabyte RAM memory and 8 processors.

All but the simplest calculations required more than one node though, either because they need more memory than which is available in a single node, or because the computational time would be unacceptably long. Thus most jobs were run in parallel, using more than one node. This in turn requires a high communication bandwidth between the different nodes, and not all clusters are designed for this purpose. Gengar is equipped with a fast infiniband connection between the different nodes and is therefore preferred for computations using more than one node. Also, in order for the different nodes to work together, a Message Passing Interface or MPI has to be utilized. MPIs are preinstalled on the cluster and require little user intervention. A script that submits jobs with an MPI is included in the appendix of this work.

VASP is designed to be executable on parallel systems, and most parts of the calculations, such as summation over the k-points, or the determination of the plane wave coefficients, can be split up and performed on multiple processors simultaneously. Several parameters influence the effectiveness of the parallelization. It is possible for instance to spread the calculations as evenly as possible between the different nodes and processors, or to try and limit the communication between the nodes to manageable levels.

Rather than optimizing these parameters, the recommendations for a "Linux cluster with multicore machines linked by a fast network" were followed, as per the VASP manual.

On a side note, during this work it occurred once that identical calculations were repeated on a different number of nodes. The number of nodes was increased from six to ten, while computational time dropped from 434 minutes to 339 minutes. This leads to a parallelization efficiency of:

$$\frac{6 \times 434}{10 \times 334} = 78\%$$

4. Goals and method

The goal of this work is twofold. The first aim is to accurately calculate the grain boundary segregation energy for a particular atomic configuration. The second goal of is to enable as much reuse as possible of the tools and methods developed during the execution of this work.

In this section the motivation an atomic scale investigation of the grain boundary energy is given, followed by a discussion on the current state of the topic in literature. Lastly, a step-by-step overview of the choice and construction of the studied system is given.

4.1. Motivation

As stated in the introduction, grain boundary segregation can have a severe impact on material properties. The segregation energy is the driving force for most types of segregation and thus systematic knowledge on the atomic mechanism behind grain boundary segregation is a valuable asset. Unfortunately, such insight on an atomic scale lies out of reach of the experiment. As an alternative, ab initio modeling is performed. Since calculations can easily be repeated for other systems once a clear procedure is developed, this work focuses on performing all necessary steps to calculate the grain boundary segregation energy for a single system and providing the reasoning and methodology behind each decision. Additionally, any useful scripts written during the execution of this work are documented and included in this text.

4.2. Other work in literature

The application of DFT to the study of grain boundaries is not new. In fact a DFT study of aluminum grain boundaries has already been carried out in 1994[28], while a 1997 work[29] mentions DFT to study impurities at grain boundaries. However, DFT remains closely associated with the field of quantum mechanics and this is reflected in the areas of its application: most papers applying DFT to grain boundaries do so for semiconductors. The focus is there much more on the properties of the band gap than on other properties. As a result, structural materials attract relatively little attention, despite a history dating back almost twenty years.

Contemporary work does exist of course. An excellent example is the analysis by Bhattacharya *et al.* of the relative stability of two grain boundaries in iron, which especially focuses on magnetic properties.[30] Work on grain boundary segregation has also been performed. A non-exhaustive study by Lejcek *et al.* compared the calculated segregation energies from dive different sources.[31] In conclusion, grain boundaries can be and are certainly described using DFT.

The availability of other work should mean that it is not necessary to start from scratch, but that existing procedures can be built on. However, reproducing reported calculations is less

than straightforward. For example, Wang *et al.* performed ab initio calculations on the cohesive energy of grain boundaries of aluminum.[32] The grain boundary was described as a tilt boundary, and a reproduction of their illustration of the boundary is shown in Figure 11.

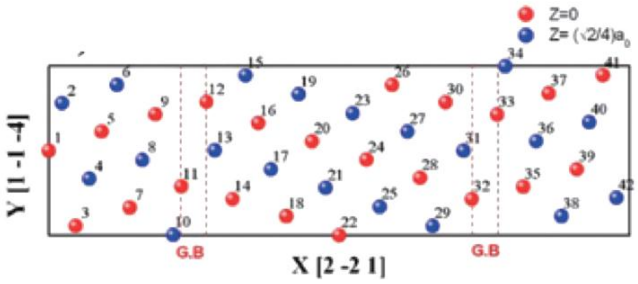

Figure 11: Unit cell used by Wang et al.[32]

Clearly, translations have broken the mirror symmetry. Also, the ideal grain boundary is modified (i.e. atoms have been removed, see further section 4.4.). This can easily be seen by the fact that there are more red atoms than blue atoms, each color representing a different (110) lattice plane. However, in the article, no information is given as to how these translations and modifications were established. Thus, anyone wishing to use a similar grain boundary will run into the same problems, if any, that Wang et al. encountered during its construction.

Additionally, the omission of such intermediate information makes it more difficult to evaluate papers. For example, a paper investigating the effects of oxygen in uranium nitride[33] depicts the grain boundary shown in Figure 12. Immediately, one can see that the grains are very far from each other, and at least one atom would easily fit in the gaps in the grain boundary. No mention is made as to why this particular configuration was used, while its properties must be undoubtedly different of those of a denser grain boundary. Whether this choice was intentional or accidental can not be determined from the paper.

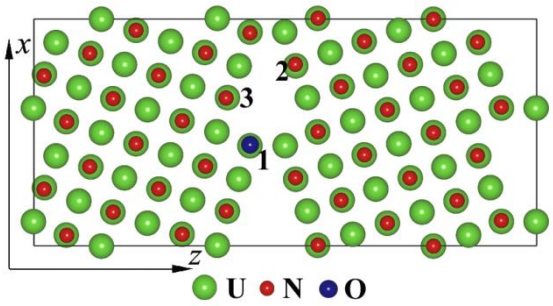

Figure 12: Unit cell used by Kotomin et al. [33]

The used parameters are another issue. The parameters are more problematic than the grain boundary configuration, since the latter can at least be easily visualized. The convergence of the main parameters for the accuracy of the result, the k-points and the cut-off energy, is often omitted[34, 35] or mentioned vaguely. The latter happening in a paper by Gao et al.[36] which mentions that further increases in k-point density caused less than one percent deviation of the total energy of the system. The total energy of a system greatly depends on the number of

electrons that are modeled, thus such a statement conveys little information except if one were to do calculations on the system as well.

The reason why so little attention is paid to convergence tests is understandable, as they do not advance towards a conclusion of a work. The situation is somewhat similar to how the calibration of a measuring instrument, if done well, has no bearing on the findings of an experiment. However, information on convergence is much more useful to the reader. A researcher wishing to reproduce certain physical measurements must always perform the same calibration on his instruments. It is therefore of little value to include extensive descriptions of calibration procedures. The situation is completely different for convergence tests. If convergence is accurately described, the resulting parameters can simply be reused for sufficiently similar calculations. This makes it easier to compare and extend existing work.

Apart from making reproduction harder, omission of the convergence tests can also make it more difficult to assess other papers. Some papers mention extremely low values for the k-point density, a study on the embrittlement of iron grain boundaries due to sulfur segregation by Sawada[37] uses 64 k-points, a twentieth of the number of used in this work, while a study on the stress corrosion cracking in nickel by Kart et al.[38] uses a mere four k-points. The question is then whether a greater error margin was accepted or whether the studied systems converged much more rapidly.

Because of the importance of reproducibility and because of the sparse description of methods in literature, a significant part of this work discusses the followed method to arrive at the final calculations.

4.3. Selection of the species

In order to pave the way for future calculations, one particular system must be considered. Copper was chosen as a bulk material because it is commonly used in pure form. Additionally it is non-magnetic, which would have compounded the calculations. The properties of copper have been well-studied, so any calculated properties can be compared to those already known.

Sulfur is known to adversely affect the mechanical properties of copper due to grain boundary segregation. At first the calculations would be performed on the segregation of sulfur in copper. However, sulfur has a very low solubility in copper. The number of atoms that can be modeled is limited, so any feasible system would be grossly supersaturated. This in turn would require great effort to isolate the effects from the sulfur atoms from each other. As the interest of this work was more in the calculation of grain boundary segregation energy, rather than specifically solving the issues for sulfur in copper, it was decided to abandon sulfur.

Instead, phosphorus was used as a segregant atom. Phosphorus has an appreciable solubility in copper and so much less problems are expected due to interacting impurity atoms. A disadvantage of phosphorus is that it does not produce the disastrous effects on the mechanical properties of copper that sulfur does, and it is thus a much less critical and less

studied impurity.

4.4. Selection of the grain boundary

A grain boundary has five macroscopic degrees of freedom. Three degrees are required to describe the misorientation between the two grains, and another two are required to describe the orientation of the boundary plane. On a smaller scale, even more degrees of freedom are possible. For example: if one grain moves less than the distance between neighboring atoms parallel to the boundary plane, the configuration at the grain boundary will change, even though the five degrees of freedom previously mentioned will remain the same. The microscopic degrees of freedom are illustrated in below.

The two figures show the atom positions along a hypothetical grain boundary perpendicular to the plane of this page. In both instances, the orientation of the two grains is identical, their coordinate systems are shown in the lower left corner. The orientation of the grain boundary remains identical as, from the bottom to the top of this page and perpendicular to it. Yet the grain boundaries are clearly distinct, as can be easily seen from the two atoms that are very close together in Figure 14 but not in Figure 13. With the five macroscopic degrees of freedom identical, it must be the microscopic degrees of freedom that differ for both figures.

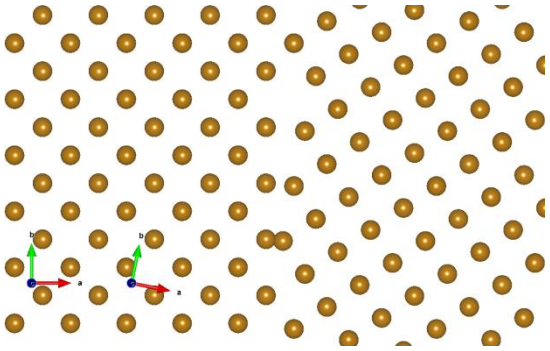

Figure 14: Hypothetical grain boundary with two atoms close

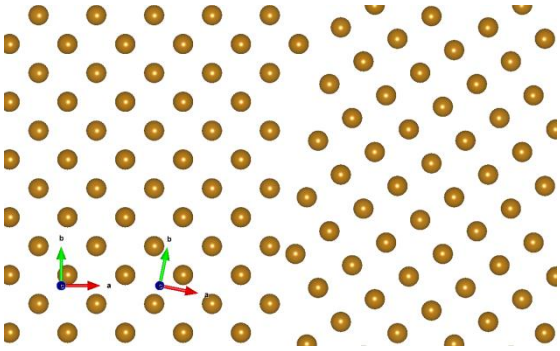

Figure 13: Hypothetical grain boundary with atoms further apart

With so many degrees of freedom, it becomes almost impossible to have a complete yet useful description of a grain boundary. And indeed, most of the time, such a complete description is not necessary. For most materials only the grain boundaries with special properties are described, other grain boundaries are simply called random. The vast majority of grain boundaries in a material is random, so it is desirable to model a representation of a random grain boundary. However, this is not possible. Due to the periodic boundary conditions used by DFT methods, only grain boundaries with small repeat units are feasible for calculations. These grain boundaries are per definition special grain boundaries.

Small repeat units imply a severe restriction on the grain boundary misorientation: if the Bravais lattices of both grains are superimposed, it must be possible to construct a space-filling repeat unit of modest dimensions. Depending on the relative misorientation between

the grains this will be possible or not. If such a repeat unit can be constructed, then both lattices can be translated in such a way that they share some lattice points in space. The points shared between two lattices form a Coincident Site Lattice or CSL. For a given CSL the misorientation between the constituent lattices is fixed. If a grain boundary is formed between two grains that are oriented in such a way that both lattices have a coincident site lattice, the grain boundary is often referred to as a CSL boundary. Figure 15 shows how two lattices can share a CSL. The yellow and blue dots belong to identical lattices with different orientations. The orientation for each lattice is shown in the lower left corner. One in five atoms of either lattice coincides with an atom in the other lattice, this is shown by the dots with two colors.

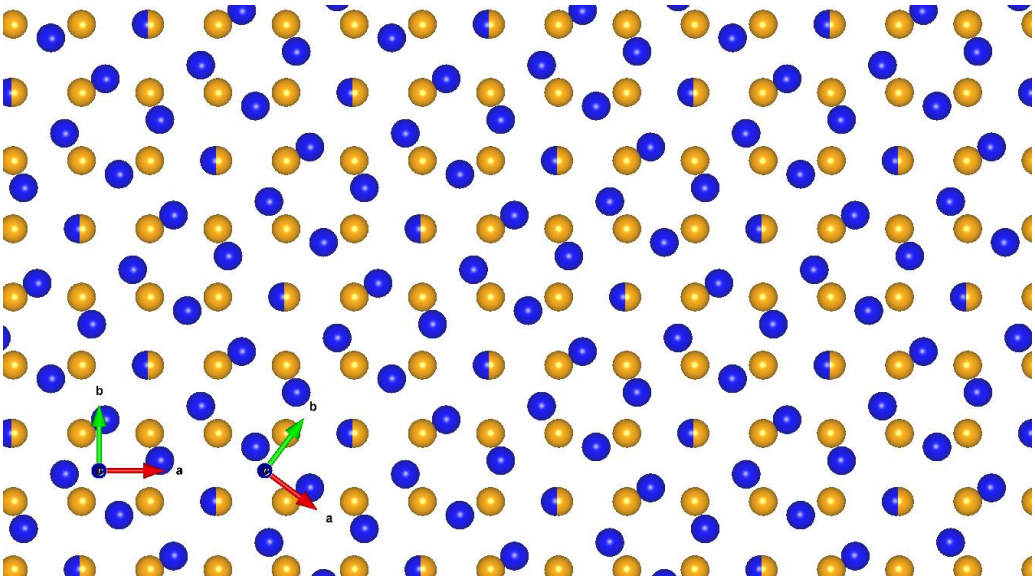

Figure 15: Illustration of a CSL

It is clear that infinitely many misorientations give rise to a CSL. Take for example a two-dimensional square lattice. Any rotation over a rational fraction of 2π will cause some lattice sites to coincide with the lattice sites before rotation. CSLs are periodic, just like the constituent lattice, although their repeat units can be much larger and of a different symmetry. To describe CSLs, Σ-values are introduced: the ratio of the amount of coincident sites to the amount of lattice points of the constituent Bravais lattice. Only small Σ-values are interesting for modeling in DFT as we wish to describe small repeat units. Figure 15 shows a grain boundary with a Σ-value of five: a Σ5 CSL.

CSLs are mostly used for cubic lattices. While a body-centered cubic lattice contains twice as many lattice points as a simple cubic lattice per unit volume, due to symmetry it will also give rise to twice as many coincident lattice points after a rotation. The same holds for the face-centered cubic lattice, with the amount of lattice points and coincident lattice points being four times as high as for the simple-cubic case. Thus a Σ9 CSL defines the same misorientation for a face-centered, body-centered or simple cubic lattice. In the case of cubic lattices, small Σ values generally uniquely define a misorientation. Larger Σ values correspond to multiple misorientations. In those cases, a Σ value alone is insufficient to define a unique misorientation. CSLs are also regularly used for hexagonal close-packed lattices.

Deviations from the perfect CSL lattices can be accommodated by the inclusion of dislocations, a kind of crystallographic defect. In this respect the Σ1 lattice is a grain boundary where all misorientation between both grains can be accommodated by dislocations. This is why these special grain boundaries occur at all in real materials. It would be extremely rare for two adjacent grains to have exactly such a misorientation that they form a perfect CSL lattice. However, the orientations must not be perfect and deviations can be tolerated up to the order of a degree. The chance that neighbors form a CSL is thus still low, but not non-existent. The boundaries modeled in this work are perfect: they exactly match the prescribed geometries.

Given a Σ-value and corresponding misorientation, the choice for the orientation of the boundary plane is often straightforward. Typically a face of the CSL repeat unit is chosen. Ideally the grain boundary contains no atoms that do not fit in both grains. The choice for the grain boundary then basically boils down to which Σ-value to take. Since most grain boundaries in a material are random, it is desirable to pick a special grain boundary with similar properties as a random grain boundary. One way to compare different grain boundaries is their energy. Since grain boundaries are crystallographic defects, they increase the energy of a crystal. The grain boundary energy per unit surface is a measure of the amount of distortion caused by the presence of the grain boundary. Random grain boundaries have relatively high grain boundary energies compared to some special grain boundaries.

While a Σ3 grain boundary has the smallest repeat unit, it also has a markedly lower energy than a random grain boundary. This can be explained by the fact that so many atoms at the boundary fit in both lattices, in effect, a Σ3 grain boundary is a twinning grain boundary. Because of this, the properties of such a boundary will be different from those found in random grain boundaries, for example the corrosion behavior. Kim *et al.* showed that the special grain boundaries were more resistant to corrosive attack than the random grain boundaries. This difference faded when the Σ-value became larger than 5.[39]

So while a very large Σ-value might seem like a good approximation of a random grain boundary, the Σ-value also should not be taken too high, as this leads to large repeat units. The Σ9 grain boundary seems to offer a trade-off: having relatively high energy among the special grain boundary and still having a low Σ-value.[40] This, combined with the availability of TEM-images of a Σ9 grain boundary[41], lead to the choice of that grain boundary for the model system in this work.

A (110) projection of a Σ9 grain boundary for a face-centered cubic material is shown in Figure 16. The fuzzy atoms have a different coordinate along the [110] axis. The structure contains two distinct (110) planes, so all atoms in the repeat unit are visible. The Σ9 grain boundary is defined by a rotation of 0.6435 rad, the arccosine of 0.8, around the [110] axis. The (2 -2 1) boundary is the logical choice for placement of the grain boundary.

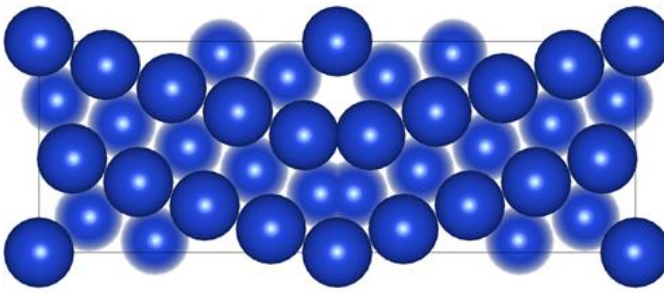

Figure 16: A Σ9 grain boundary

A perfect Σ9 grain boundary contains some atoms that are very close together. The original idea was to solve this by relaxation. However these atoms are too close together for accurate calculations so there was no starting point for relaxation. A modified Σ9 grain boundary has one of the two atoms that are very close together removed. A modified and a standard Σ9 grain boundary are compared in Figure 17. The yellow atoms are removed from a modified grain boundary.

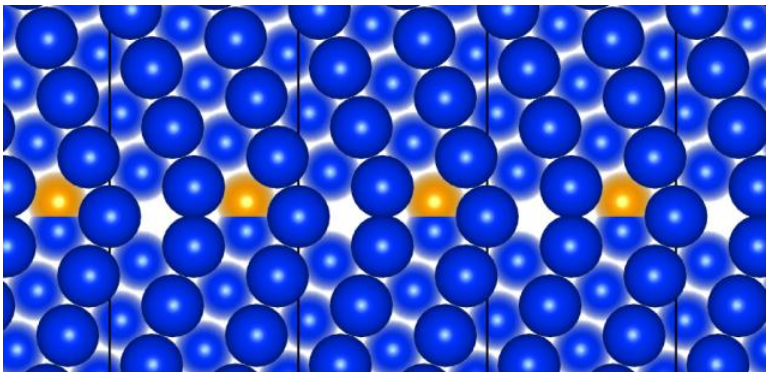

Figure 17: Comparison between standard and modified Σ9 grain boundaries

Hu et al. observed a modified Σ9 grain boundary along with a boundary with a grain boundary energy of 756 mJ/m².[42] This is shown in Figure 18. The kite-like formations are modified Σ9 grain boundaries, while the other type of grain boundary in the top of the picture was found to have the mentioned energy of 756 mJ/m². Since this is a relatively high value for a grain boundary energy, it was decided to work with a modified Σ9 grain boundary under the assumption that the modified grain boundary would exhibit a similar energy.

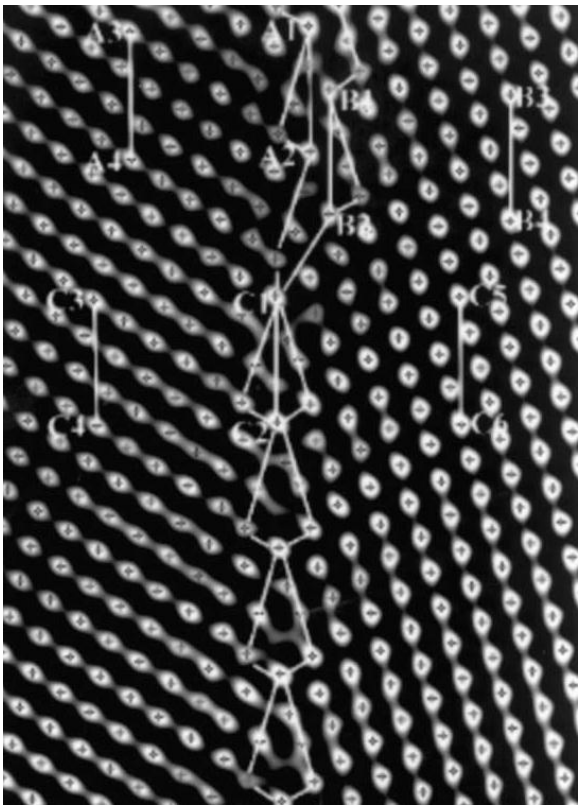

Figure 18: Image from the work of Hu et al.[42]

With the choice of a Σ-value and a grain boundary orientation, the five macroscopic degrees of freedom are fixed. To account for the microscopic degrees of freedom, relaxations must be performed. The relaxation procedure will be given later in this chapter.

4.5. Supercell construction

As described previously the POSCAR file contains the description of the unit cell that is repeated in space. For bulk solids these unit cells are very small. Most primitive cells for crystals contain only a few atoms. However, if a more complex structure needs to be modeled, tens or even hundreds of atoms must be included. To make the distinction with a smaller cell, the term supercell is often used. A grain boundary is an example of a system that is described by a supercell.

The first step when given a Σ-value for a cubic system is to look up around which axis rotation happened. Tables for cubic and hexagonal systems are widely available. Then the crystallographic plane perpendicular to this rotation axis can be determined. Since the misorientation is the same for body-centered, face-centered and simple cubic lattices, it is easier to work for a simple cubic lattice with lattice parameter one.

With the lattice points in the plane perpendicular to the rotation axis, it is possible to obtain the rotation angle corresponding to the Σ-value and then the positions of the Coincident Site

Lattice. This can be done with elementary trigonometry, but writing out the equations out for the general case becomes quite messy. Since we are concerned with low values for Σ, trial-and-error is much faster. Additionally most sources that mention the rotation axis also mention the rotation angle.

When the two dimensional CSL and the rotation angle are known, only one additional piece of information is required to construct a supercell containing the boundary: the repetition along the rotation axis. For example, in the simple cubic lattice with rotation axis [110] the distance between two (110) planes is $\sqrt{2}/2$ times the lattice parameter, but two subsequent planes have undergone a translation parallel to the (110) plane so the system is periodic along the (110) axis with period $\sqrt{2}$ times the lattice parameter.

After a supercell is constructed, it can be reduced in size. In principle, a CSL unit does not need to contain more than its Σ-value in atoms. However this cell with the least amount of atoms is not necessarily cuboid and such cells are much easier to work with. Therefore cells larger than this bare minimum are commonly used. This has the additional advantage that if impurities are added to the cell, they are diluted more and that for some geometries the grain boundaries are further removed from each other. Two unit cells of the CSL lattice, each containing one of the two orientations of the Bravais lattice, can easily be concatenated to form an even larger supercell containing the grain boundary. The supercell is constructed in such a way that its repetition in space forms a layered structure: the orientations before and after rotation are stacked on top of each other and each interface forms a grain boundary. As a result, there are two grain boundaries per super cell.

A Matlab script that constructs this supercell when given the rotation axis, rotation angle and the lattice vectors of the CSL perpendicular to the rotation axis is included in the appendix of this work. This script works on the files used by the Wien2k software program to store crystallographic information. These Wien2k files can easily be converted to and from files readable by VASP in the POSCAR format. The Matlab script uses functions that are included in the Wien2k package to perform elementary operations on the input files. The original crystallographic data was obtained from the Crystallographic Open Database[46] .

The supercell that was used in this work contains 36 atoms. Two atoms are removed to modify the two Σ9 grain boundaries in the cell, resulting in 34 atoms for the supercell containing the grain boundaries. The cell is cuboid, and has mirror-symmetry around the grain boundary. The grain boundaries are perpendicular to the c-axis and are located halfway the cell and at its edges. A .cif file is included in the appendix of this work that contains a full crystallographic description of the unit cell.

Another approach to construct the supercell would have been to include a vacuum in each cell so that only one grain boundary is included. Working with a vacuum does take extra precautions though, because it can easily introduce errors. Also, a free surface would arguable influence the nearby copper atoms more than a grain boundary, so the vacuum approach was discarded.

4.6. Relaxation procedure

VASP allows for the relaxation of atoms, cell shape and cell volume. However relaxations that alter the cell are not without difficulty. Because the plane wave basis set depends on the geometry of the cell, alteration of the cell shape can influence the result of the calculations, especially the values of the stress tensor. This phenomenon is called the Pulay Stress.[25] The Pulay Stress is almost isotropic, so changes that conserve cell volume are much less affected. The relaxations necessary for the Σ9 copper system require changes in both shape and volume. The effects of the Pulay stress were completely avoided however. Calculations were repeated for fixed volume, and for each volume a new plane wave basis set was created based on a cut-off value. The energy for each volume was then interpolated to find a minimum.

The followed relaxation procedure is non-standard for several reasons. First only the atoms near the two grain boundaries in the cell were allowed to relax. This was done because the distance between the grain boundaries was only three times the lattice parameter of the face-centered cubic copper lattice. A grain boundary is expected to influence the lattice much farther than that distance. Hence, if all atoms would be allowed to relax, then the resulting structure would be markedly different from bulk copper. By fixing the atoms that are not directly adjacent to the grain boundary, at least those atoms remain in the same configuration as the one in pure bulk copper. This way the performed calculations should bear a better resemblance to the properties of bulk copper.

Since the distance between the atoms not adjacent to the grain boundary was fixed, there could be no change in dimension of the unit cell in directions parallel to the grain boundary. Additionally, all change in dimension perpendicular to the grain boundary would have to be completely accommodated by the grain boundary itself. The material between the grain boundaries has to remain unchanged to keep the bulk configuration. Figure 19 illustrates this relaxation scheme. The elongation has been exaggerated to show clearer how only the grain boundaries accommodate the elongation.

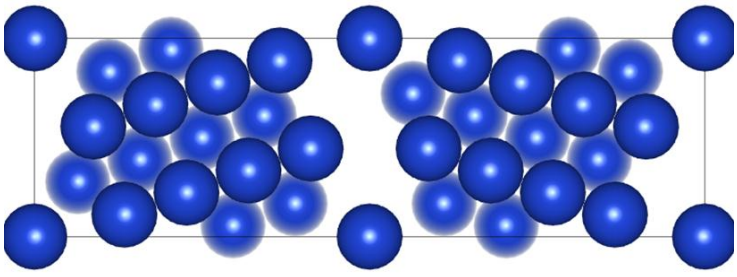

Figure 19: Elongated unit cell

Lastly, from the High-Resolution Transmission Electron Microscopy images by Hu *et al., see* Figure 18, it is apparent that the modified Σ9 grain boundary retains mirror symmetry on the boundary plane. Hence the grains were not allowed to move relative to each other in a way that would break this symmetry. In effect the only movement allowed is the one included in the volume relaxation.

4.7. Calculation of segregation energy

After the supercell containing the grain boundary is fully relaxed, calculations on the segregation energy of phosphorus can begin. The segregation energy is defined as the difference between the energy of an impurity atom in the bulk of a material and the same impurity atom at the grain boundary of the material. The unit cell describing the grain boundary contains no true bulk material, since the influence of the grain boundaries is felt throughout the cell. The area between the two grain boundaries has the same lattice configuration as the true bulk material though. This bulk-like environment of the supercells containing a grain boundary will be referred to as pseudobulk in the remainder of this work.

To calculate the energy of an atom in the bulk of the material, supercells are created where the copper atom in the pseudobulk is replaced by a phosphorus atom. For the energy of the phosphorus atom near the grain boundary, supercells are created where a copper atoms near the grain boundary is replaced. It was also noted that the relaxed grain boundary structure contains a relatively large hole. In a last supercell, a phosphorus atom was placed in this hole, as shown in Figure 20. The other sites are shown in Figure 21, each of the numbered atoms is one of the positions where a phosphorus atom is placed substitutionally.

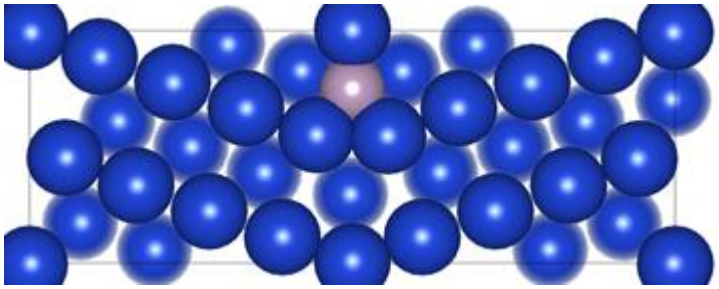

Figure 20: A relaxed cell, showing the location of the interstitial position

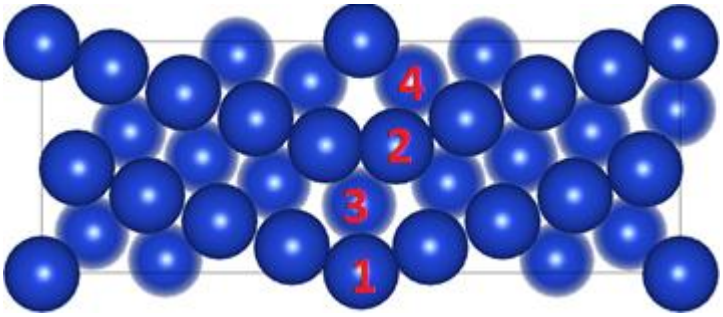

Figure 21: The four substitutional positions

5. Results

This chapter will give an overview of the performed computer calculations and their results. First the preliminary calculations will be discussed. These calculations were necessary to obtain the necessary parameters of the final system. Then the calculations of the physical properties of the system are discussed, including the segregation energy. Lastly, a note on the accuracy of the calculations is given.

5.1. K-points convergence

It is established that the amount of k-points is critical for the success of calculations. Too few k-points will give inaccurate results, while too many k-points are an unnecessary strain on computing resources. K-points are also very dependent on the geometry of the cell, so it is difficult to use guidelines. Instead, convergence tests should be carried out for each type of cell. A convergence test consists of steadily increasing the amount of k-points until the result of the calculation does not vary anymore with a further increase. Typically a doubling in the number of k-points is needed to obtain a noticeable effect. In the tests, the number of k-points was not exactly doubled at every step, this was done in order to maintain an k-point grid that is as uniform as possible.

The number of k-points that could not be mapped to others with symmetry operations (the number of irreducible k-points) was 25%-33% of the total number of k-points for all studied cells. Cells with fewer k-points had a higher percentage of irreducible k-points which can be intuitively understood from edge effects. Certain k-points such as the Γ point at the origin of the Brillouin zone can never be mapped to other k-points. The sparser the mesh, the more important these edge effects become.

For the k-point convergence, the total energy of the system was used. In principle each property of the system should be tested for convergence: it is for example entirely possible that the total energy has converged but the pressure on the system has not. Since this work is almost exclusively concerned with energies, convergence was carried out exclusively for the total energy.

Note that in the graphs below, the convergence is plotted, not the total energy of the system. The graph displays the difference between the calculated value and the calculation with the most stringent parameters for that system.

In order to be able to compare two cells with and without a grain boundary, a supercell was constructed with the same dimensions as the grain boundary supercell, but containing only a single copper lattice. This copper lattice was oriented in the same way as one of the two grains of the grain boundary supercell. The supercell without the grain boundary was called the bulk cell. Both the modified and the standard grain boundary were included in tests.

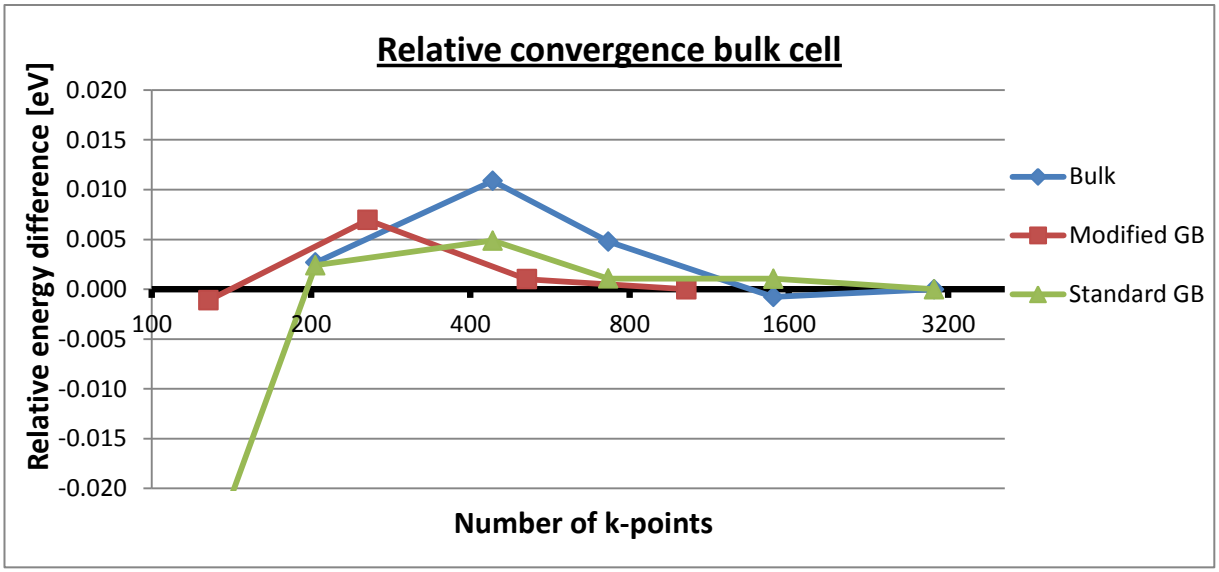

Graph 1: k-point convergence

Convergence of less than 1.5 meV for the modified and the standard grain boundary is achieved for 512 and 729 k-points respectively. The convergence for the bulk cell is slower, requiring another doubling of the k-points to 1496. But then good convergence has been achieved as well: the difference between the result for 1496 and 3010 k-points is only 0.8 meV. Hence, all future calculations used 1496 k-points.

To illustrate the effects of increasing the number of k-points on the computing requirements, the graph below shows the computational time needed for each amount of k-points for the bulk cell. To correct for parallelization, the elapsed time of the calculation is multiplied with the number of processors used. The time is thus expressed in processor-hours.

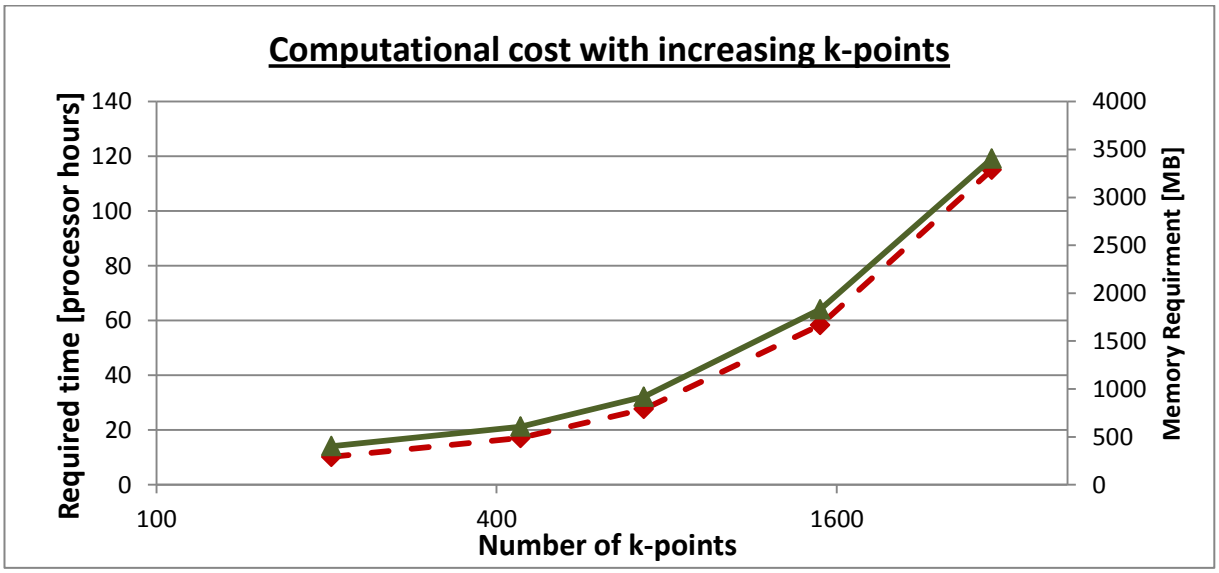

Graph 2: k-point computational scaling (the dashed curve maps to the left)

A single processor would need almost 120 hours to complete the 3010 k-point calculation on a bulk cell, this is five days. The memory requirements scale virtually identical to the time requirements. For the 3010 k-point calculation 26.4 gigabyte of memory was used, for the 204 k-point test 3.13 gigabytes sufficed.

5.2. Convergence of the basis set

Another critical parameter for the success of the calculations is the size of the basis set. The size of the basis set is determined by the cut-off. Since each plane wave in the basis set has an associated energy and waves with higher energy generally have smaller coefficients and contribute less to the approximation to the real Kohn-Sham orbitals, the cut-off point is given as an energy level.

There is a minimum cut-off below which the PAW-method will break down. This minimum depends on the exact method by which the PAW-basis was calculated and is supplied alongside with it. For the PAWs used in this work, the minimal cut-off was less than 300 eV. All used energies are above this minimum.

Convergence is tested differently for the cut-off energy. Rather than looking at the total energy of the system with increasing cut-off energy, one has to look at the energy difference between two similar systems. In this case the energy difference was used between the bulk cell and the bulk cell with a 5% increased lattice parameter.

In the graph below, the convergence of this difference (called discrepancy in the graph), which was 3.40 eV, is plotted.

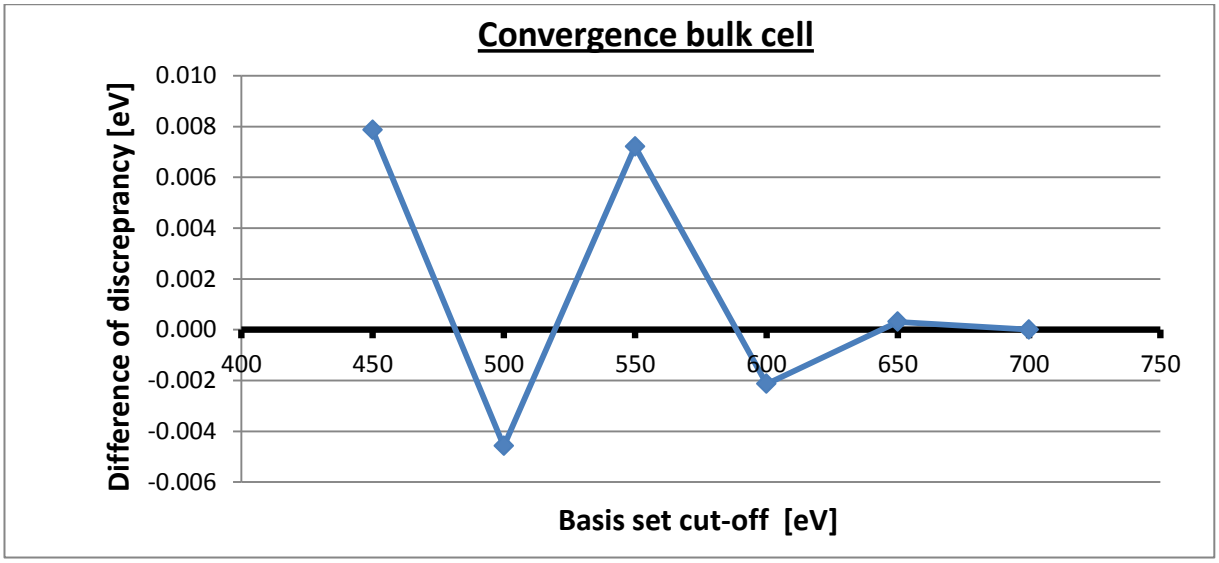

Graph 3: Basis set convergence

Convergence to 2 meV happens for a cut-off energy of 600 eV. Unfortunately, due to human error, the optimal cut-off was determined to be 550 eV. Thus, convergence was only carried out to 8 meV. The 6 meV in accuracy that has been lost this way is a setback, but does not

affect the conclusions of this thesis too much. After all, while calculations should be as accurate as possible, an uncertainty of several meV for the whole cell is acceptable for the purposes of calculating a segregation energy.

Again, an increase in cut-off level increases computational time and memory use. Below the computation time is shown as a function of the cut-off energy. To correct for parallelization, the elapsed time is multiplied by the number of processors. The time is thus expressed in processor hours.

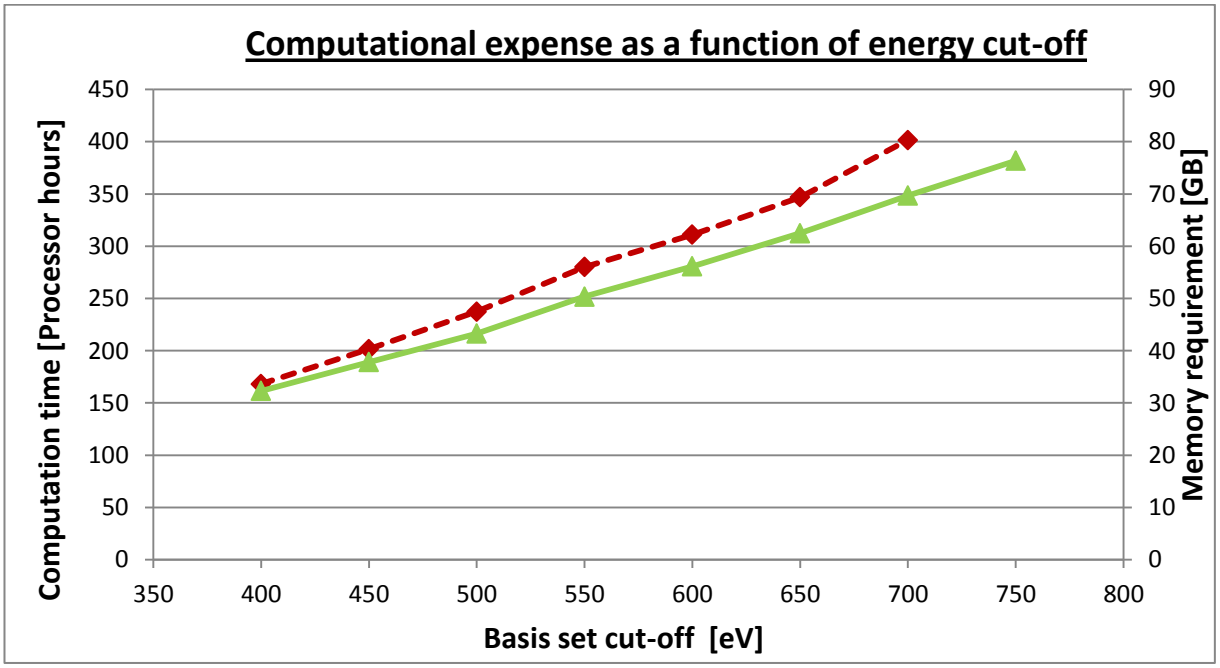

Graph 4: Basis set computational expense (the dashed curve maps to the left)

Unlike for the k-points, a linear relationship is seen between the cut-off energy and the computational expense. For the highest energy cut-offs, a single processor would need 400 hours or more than 16 days to converge to the solution.

Note that the 750 eV cut-off is not included. The system ran out-off virtual memory while writing out the electronic configuration of the system to the hard disk. This work did not use the electronic configuration from the convergence tests so the crash did not affect the relevant calculations, but as a result the run-time was shortened to about 400 processor hours, the same value as for a 700 eV cut-off. The reason why the electronic structure is written at all even if it is not used is because it allows calculations to continue with the system. Just as for the k-points convergence, the memory requirement follows the same trend as the computation time, with the time rising just a bit faster.

5.3. Independence of basis set and k-points

Until now it has been aptly assumed that convergence of k-points and the cut-off energy for the basis set is independent. To test this, two values were chosen for the k-point density that

had converged according to the k-point convergence tests: 1496 k-points and 3010 k-points. Then several cut-off energies were used in combination with both those k-point densities. The results are shown below.

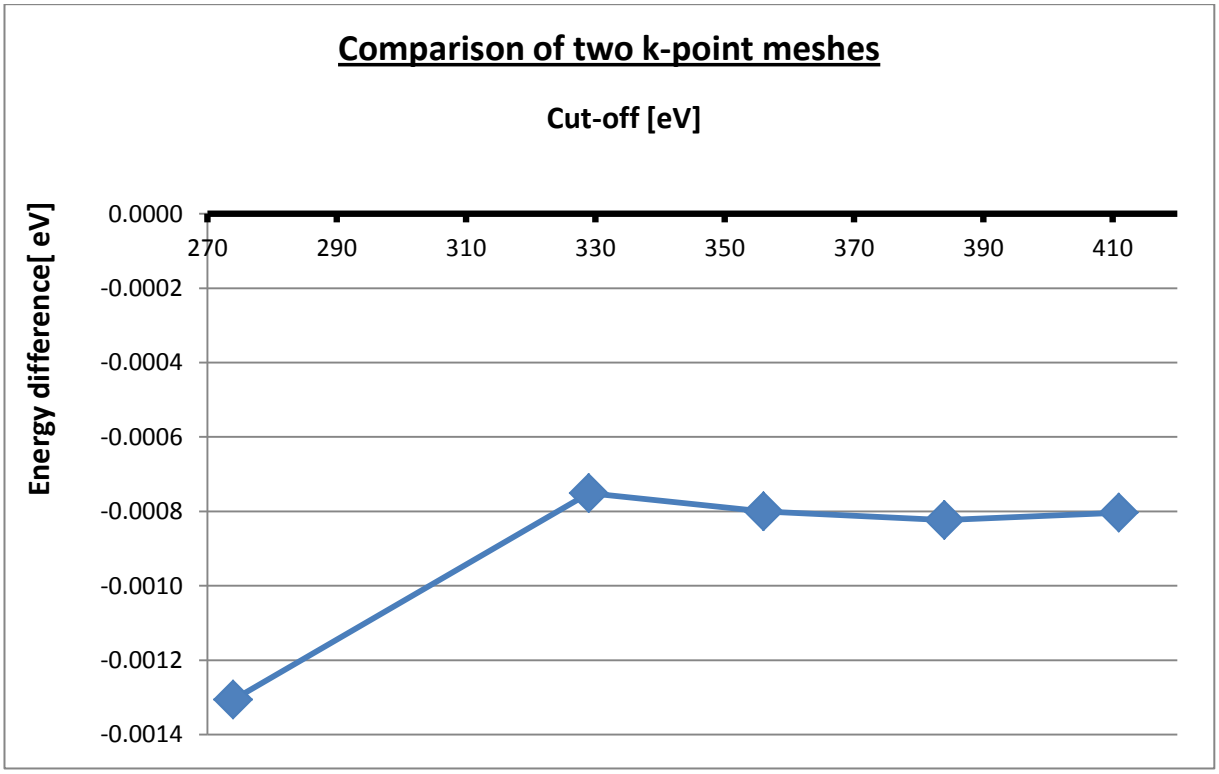

Graph 5: Basis set variance for two k-point meshes

Both meshes obtain very similar results. The difference is of the order of 1 meV so the convergence of the k-points seems to be independent of the cut-off energy.

5.4. Energy of the free atom

For comparison, it is useful to know the energy of the free atoms that were used in the calculations. With this energy, the values of the cohesive energy of copper and the energy gained by dissolving phosphorus in it can be obtained. Strictly speaking, this energy is not necessary for calculating the segregation energy in copper, since this energy is calculated as a difference between the energy of the system with phosphorus in a location far from the grain boundary and in a location near the grain boundary.

Calculation of the energy of a free atom is relatively straightforward: a single atom is placed in a huge and otherwise empty unit cell. Care must be taken that the cell in question is large enough so that there is negligible interaction between the repeated atoms. Also, according to the VASP manual, only one k-point, the Γ point should be used as a k-point. Finally, the smearing method should be Gaussian, instead of the default Methfessel-Paxton method and the default sigma should be halved to 0.1.

Calculations have been performed for both phosphorus and copper. For each species, different cell sizes were used so that relative convergence against the cell size could be checked.

For copper, the lattice parameter of a face-centered cubic cell was repeatedly increased.

Table 1: Calculations on free copper atom

Lattice parameter [nm]	Factor from standard	Total energy [eV]	Deviation from largest [meV]	36 deviations [meV]
4.0	11	-0.06524	-0.02	-0.58
4.3	12	-0.06515	0.07	2.55
5.1	14	-0.06522	0	0

For the phosphorus atom the lattice parameter of a simple cubic cell was increased.

Table 2: Calculations on free phosphorus atom

Lattice parameter [nm]	Total energy [eV]	Deviation from largest [meV]	36 times deviation [meV]
2.0	-0.18298	-0.06	-2.23
2.8	-0.18292	<0.001	0.002
3.6	-0.18291	0.01	0.33
4.4	-0.18299	-0.07	-2.68
4.8	-0.18299	-0.07	-2.64
5.2	-0.18292	0	0

The smallest cells were big enough to eliminate the interaction between the atoms, so no convergent trend is observed. The difference between the different measurements can then be assumed to be the error on the calculations. This error is multiplied by 36 to give an idea of what the cumulative effect would be on the supercells used in this work. This cumulative effect seems to be on the order of 3 meV, which is comparable in magnitude to the convergence of the cut-off for the basis set.

5.5. Lattice parameter of bulk copper

Since several approximations are made in the DFT method, the calculated values are slightly different from the values in reality. It is known that the used PBE-potential tends to overestimate the volume slightly.[43] Subsequently, if the lattice parameter obtained by experimentation would be used for calculations, the modeled system would include a rather large hydrostatic pressure to cancel this overestimation out. Since such a large pressure is undesirable, the lattice parameter will be used that corresponds to the zero external pressure according to the DFT model.

As explained elsewhere, volume relaxations are problematic due to the Pulay Stress. Therefore another method will be used. The energy of the system will be calculated for several lattice parameters. This way a scatter plot of energy versus volume is obtained. Then an interpolation can be made to find the volume corresponding to the lowest energy. The lattice parameter of this volume is the sought lattice parameter for further calculations.

The calculations were performed for a primitive face-centered cubic unit cell. Since this cell contains only one atom and a high-level of symmetry, calculation times are extremely short, in the order of minutes on a single node. It is therefore not as critical to select the lowest possible value for k-points and energy cut-off. A lattice consisting of 110592 k-points was selected after convergence to 3.4 10^{-5} eV. The energy cut-off was taken at 356 eV, after achieving convergence to 3 meV.

The method of interpolation from the measured energy-volume points has to be very accurate and insensitive to noise though. A good way to do this is by using a model that already contains information on the system. The third-order Birch-Murnaghan equation of state is such a model. This model approximates the derivative of the bulk modulus to the pressure as a constant. Fitting to the equation of state was performed by the built-in Matlab routine for non-linear regression. This routine uses the Levenberg-Marquardt algorithm. Given the points that must be fitted and the model the algorithm iteratively searches for the model parameters that minimize the squares between the calculated values and the model. Since all parameters of the Birch-Murnaghan equation of state have physical meaning, the results can be compared to known data. The script used for the fitting is available as an addendum. It requires a license for Matlab and its statistics package.

In the graphs below, the Birch-Murnaghan equation of state with fitted parameters is plotted along with the calculated data points.

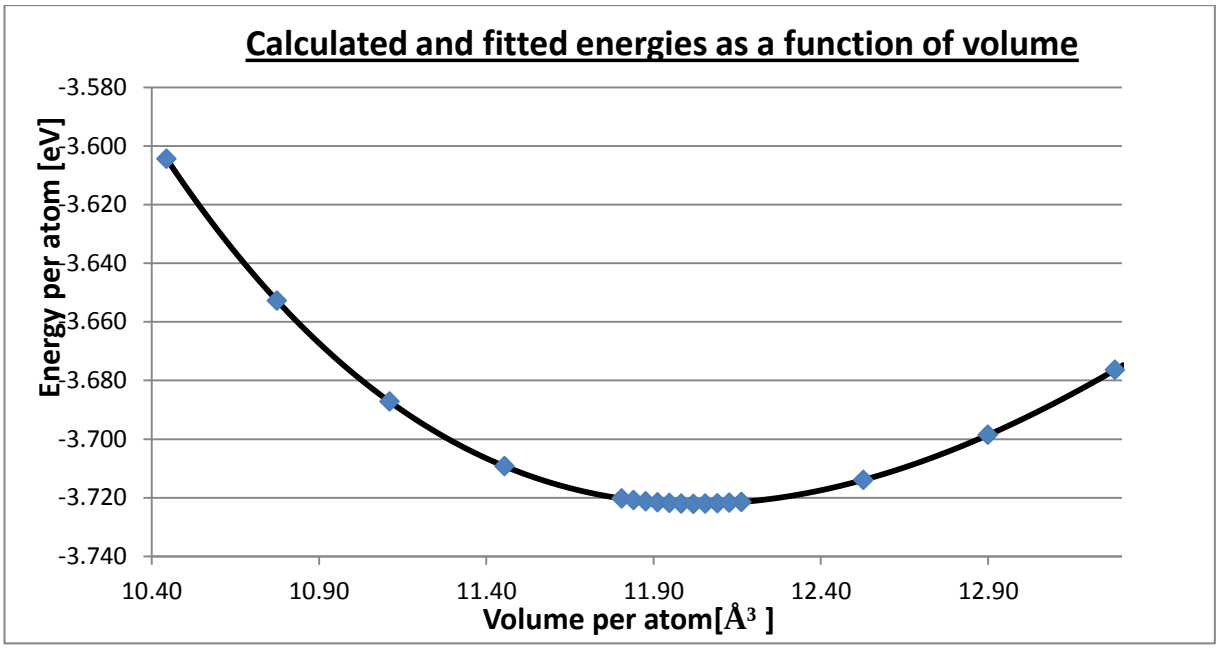

Graph 6: Birch-Murnaghan fit on copper

Since the main interest lies in determining the volume corresponding to the lowest energy, below a detail is shown from the graph above.

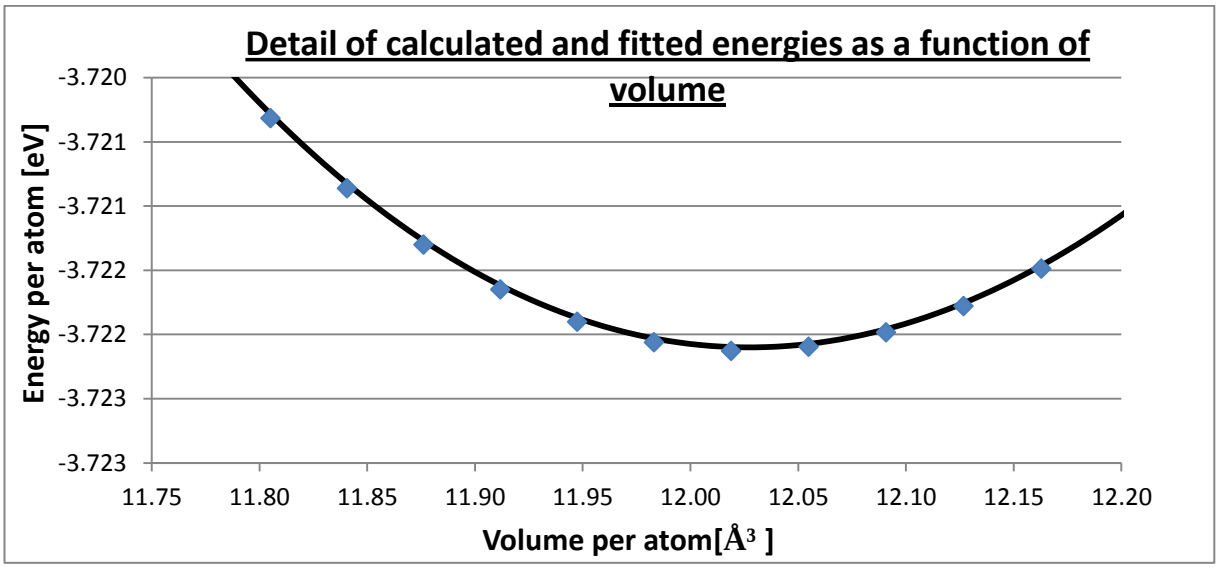

Graph 7: Detail of Birch-Murnaghan fit for copper

The average of the squared differences between the fit and the calculated energies, the mean squared error, is 2 10^{-8} eV, for comparison, the mean squared error for a quadratic fit obtained by multiple linear regression was 7.6 10^{-6} eV. A clear indication of the power of using a fitting function that contains information about the system.

The fitted parameters of the Birch-Murnaghan equation are the first calculated result that can be compared to experimental values. This is done in the table below.

Table 3: Fitted parameters of copper

	Fitted	**From experiment at 298 K [17]**
Minimum energy total system [eV]	-3.7221	
Volume per atom [Å³]	12.027	11.810
Corresponding lattice parameter [Å]	3.637	3.615
Bulk modulus	0.8538 eV/ Å³ or 136.79 GPa	133
Pressure derivative of the bulk modulus [-]	4.962	5.300

The overestimation of the volume is typical for the used PBE functional. Strangely, the pressure derivative of the bulk modulus is underestimated, while the PBE functional tends to overestimate this as well. The deviations are nothing unexpected though, less than a percent for the lattice parameter.

5.6. Relaxation of supercell

After construction of the supercell containing the grain boundary, the optimal distance between the two grains has to be found. Again, the energy of the system will be calculated for several discrete values of displacement and then a minimum will be sought by interpolation. Since all movement of the grains has to be accommodated in the grain boundaries, new atomic configurations have to written for each displacement. This is done by changing the axis of the supercell perpendicular to the grain boundary. The cell is not stretched though, so the relative configuration of the atoms remains unchanged, the atoms are only moved closer or further from the grain boundaries. The same script that is used to construct the supercell can be used to perform these actions. Since the modified Σ9 grain boundary has one atom less than the perfect Σ9 boundary, it is expected that the two grains will have to be moved closer together. Relaxation is compounded by the fact that for each displacement the atoms must be again allowed to relax, this makes these calculations very time-consuming.

Since the compression happened in a grain boundary, the Birch-Murnaghan equation of state does not hold and loses its information advantage over other fits. This can easily be seen by the fact that the mean squared error was no better for the Birch-Murnaghan equation of state than for a simple second-order polynomial. For simplicity, the polynomial fit was used to determine the optimum displacement. Fitting was done by multiple linear regression in Microsoft Excel. The graph below shows the calculated energies and a quadratic fit.

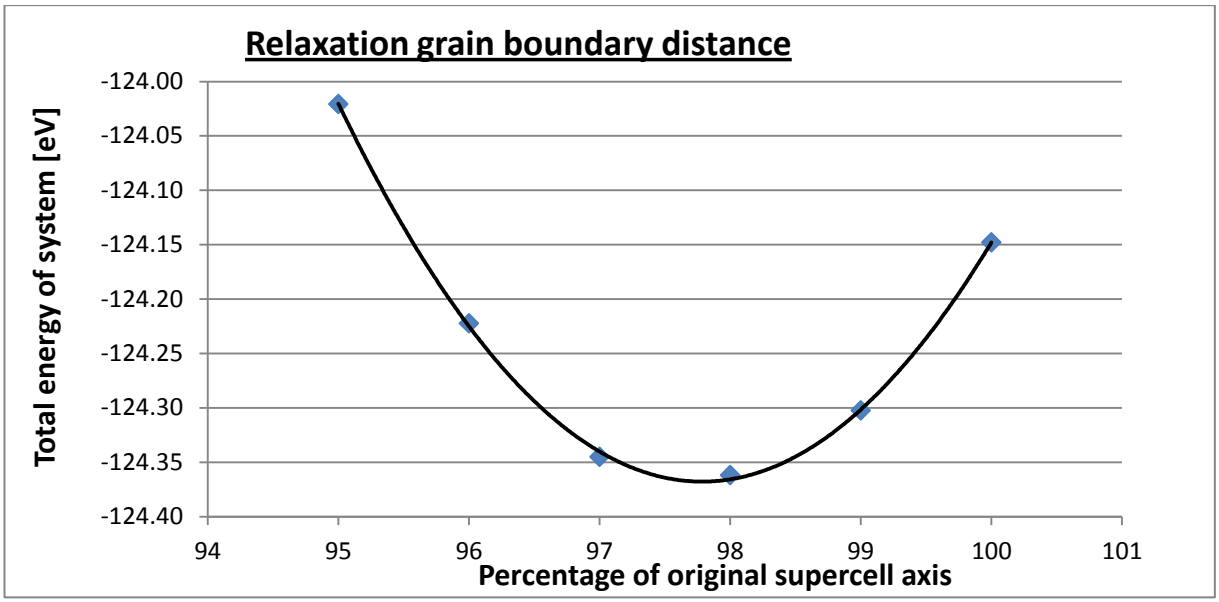

Graph 8: Relaxation of grain boundary distance

The optimal displacement was found to be when the supercell axis was 97.785% of its original value. This results in a structure that is less dense than bulk copper since it contains two atoms less. The volume per atom is 103.54% of that given in Table 3. The mean squared error for the quadratic fit is $8\ 10^{-6}$ eV, while it was $5\ 10^{-6}$ eV for the Birch-Murnaghan fit.

5.7. Cohesive energy of copper

Taking into account all the parameters obtained before, it is possible to start calculations on the physical quantities of the system. This is also the first opportunity to check calculated values against known physical quantities. A first such check is the cohesive energy of pure bulk copper since we can obtain this value from two sets of calculations.

From previous calculations we know that the energy of a free copper atom is -0.0652 eV in VASP. From the Birch-Murnaghan fit it is known that the total energy per atom in bulk copper is -3.722 eV. Subtracting the energy of the free copper atom results in a cohesive energy of -3.657 eV.

Also, convergence tests have been carried out on a bulk cell containing 36 atoms. The total energy of this system was -133.865 eV. Subtracting 36 times the energy of the free atoms gives -131.518 eV or -3.653 per atom. This is a difference of less than 0.1%, suggesting that relative convergence had been achieved for both the settings of the bulk cell and for the settings of the unit cell with one copper atom.

Additionally, this value can be compared to that of the experiment. Kittel[44] mentions an experimental value of 3.48 eV/atom. This means VASP overestimates the cohesive energy by 5%. This is an acceptable result, although it is also an indication of the difference between the DFT calculations and the real values. Interestingly, Lejaeghere *et al.*[43] also performed a DFT calculation for copper with very similar parameters and obtained 3.47 eV/atom. This was

done by taking into account the systematic overestimation by DFT for all elements. However, a systematic correction is less useful for this work, as we are interested in the difference between two calculated values and the correction on both values would largely cancel each other out.

5.8. Grain boundary energy

A second property to be investigated is the grain boundary energy. Since the goal is to approximate a random grain boundary, it is hoped that the grain boundary energy for our system is comparable to that of a random grain boundary. From the relaxation of the supercell, the total energy of the system with a grain boundary was -124.37 eV. This energy is for only 34 atoms though, as opposed to the bulk cell that contains 36 atoms. Correcting for this we obtain:

$$-124.368\ \text{eV} + 133.865.\frac{34}{36}\text{eV} = 2.060\ \text{eV}$$

Each cell contains 2 grain boundaries, of each 19.72 Å². This results in an energy of 0.0522 eV/ Å², or 0.837 J/m². This value is ~10% higher than experimental values, but shows good agreement with other ab initio calculations on special grain boundaries.[45] As such the primary goal of the grain boundary selection is fulfilled: a boundary was chosen with high, but reasonable, grain boundary energy.

5.9. Free phosphorus to bulk copper

Another interesting calculation is the energy that is needed to bring a phosphorus atom in the bulk phase substitutionally and make the displaced copper atom a free atom. Again we can calculate this value with two systems, allowing an insight in the convergence properties. First the pure bulk cell containing 36 copper atoms was considered.

In this cell, one copper atom was substituted for copper. This calculation gave a total energy of -135.226 eV. From this and the previously known cohesive energy of copper it is possible to calculate the solution enthalpy of phosphorus in bulk copper.

$$-135.226\ \text{eV} + 133.867\ \text{eV} = -1.359\ eV$$

One free phosphorus atom is introduced (energy: -0.1830 eV) and one free copper atom leaves the system (energy: -0.06522 eV), resulting in

$$-1.359\ eV + 0.1830\ eV - 0.06522\ eV = -1.241\ eV$$

5.10. Comparison pseudobulk and bulk

The same can now be calculated using the pseudobulk environment of the supercell containing a grain boundary instead of a pure bulk cell. The system then has to be compared

with a pure grain boundary cell.

Table 4: Pseudobulk results

Position	Total energy [eV]	Energy difference with GB cell [eV]	One free copper atom less in system [eV]	Correction for free energy of phosphorus [eV]	Difference with bulk supercell [eV]
Bulk 1	-125.745	-1.378	-1.443	-1.260	0.019
Bulk 2	-125.737	-1.370	-1.435	-1.252	0.011

A difference of 0.015 eV is an excellent result. It is clear that the presence of grain boundaries in the cell has some influence, but this influence seems to be rather limited as the phosphorus atoms feel a very similar environment in the bulk and pseudobulk.

This can also be seen from the electron densities. The difference in electron density for the grain boundary cell and the bulk cell is a measure for how far the influence of the grain boundary is felt in the cell. In Figure 22 the isosurfaces of density difference of ± 10^{-3} electrons per nm^3 are plotted. The red areas are intersections of isosurfaces with the viewing plane, the black spheres represent atom positions. The grain boundaries are located on the left and right edges of the figure

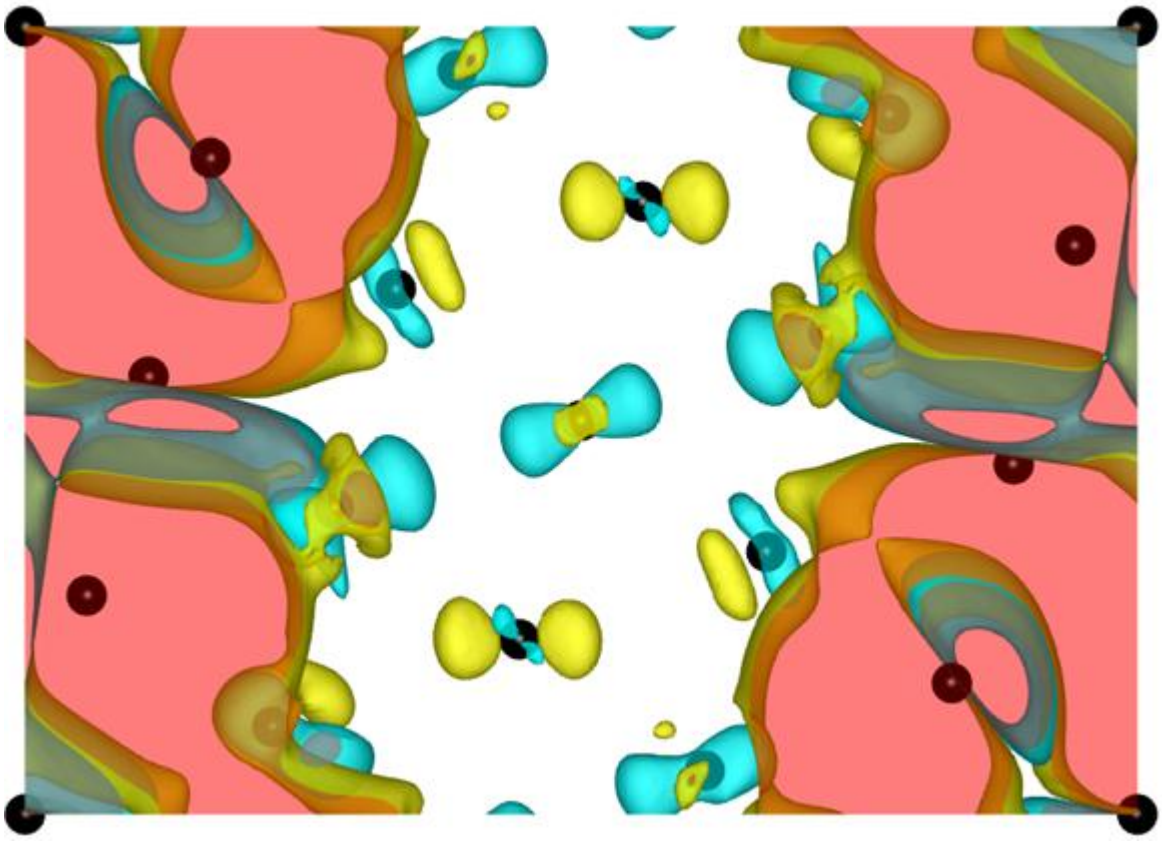

Figure 22: Isosurfaces of the difference in valence electron density

Although the influence of the grain boundary is clearly felt throughout the unit cell, there is a relatively large area where the difference in electron densities is less than 10^{-3} electrons per nm³. For comparison, the average valence electron densities are 864 and 915 electrons per nm³ for the boundary and bulk cells respectively, although this concentration is mainly concentrated around the nuclei.

5.11. Segregation energy

Lastly, the segregation energy can be calculated. Taking into account all calculated values above such as lattice parameters and relaxation, several cells are created. Four cells have the phosphorus atom in a grain boundary environment, where it substituted a copper atom. Additionally, one cell was constructed that did not replace any copper atoms, but contained the phosphorus atom in a hole on the cavity.

From the total energy of these cells, the grain boundary segregation energy can be calculated. This is done in the table below. The segregation energy is by definition the difference in energy between a system with phosphorus on the grain boundaries and phosphorus in the bulk of the material. The latter being approximated by a pseudobulk cell. A negative segregation energy means that a position at the grain boundary is energetically favored. As a reminder, the atom positions are repeated in Figure 23.

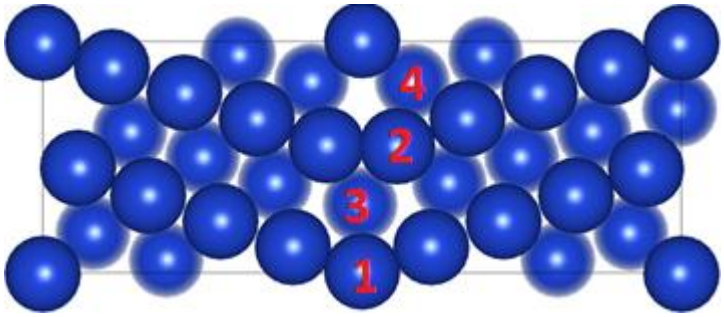

Figure 23: Substitutional postions in the grain boundary

Table 5: Calculation of segregation energy

Position	Total energy [eV]	Energy diff. with pseudobulk [eV]
Boundary 1	-126.329	-0.588
Boundary 2	-126.208	-0.466
Boundary 3	-125.693	+0.049
Boundary 4	-125.916	-0.175
Interstitial	-129.162	-3.420 (not segregation energy)

The values in the last column are the segregation energies except for the interstitial position. Since this last system contains one more copper atom, this must be somehow be corrected for. The most conservative correction is to subtract the total energy of a copper atom in bulk. This gives a segregation energy of +0.298 eV.

The difference between the different atoms in the grain boundary is striking. Two positions are relatively favorable for phosphorus, while the other two are not. At first sight, positions 1 and 3 have more in common, as they both lie centrally on the grain boundary. However, after some investigation it has been found that the distance to the closest neighbors correlates markedly with the grain boundary segregation energy. This is shown in Table 6. Due to the periodic nature of the cell, each atom has two neighbors at exactly the same distance. This degeneracy is not listed. The distances mentioned in Table 6 are for the non-relaxed atoms. The energies in Table 5 however are from the relaxed system. The relaxation only lowers the energy of the system with a couple of meV except for the interstitial system where relaxation lowered the energy with several eV..

Table 6: Distance to neighbors for substitutional grain boundary positions, before relaxation, in Å

Position	Distance to closest	Distance to second closest	Distance to third closest	Distance to fourth closest	Distance to fifth closest
1	2.452	2.457	2.521	2.522	2.576
2	2.365	2.486	2.526	2.567	2.641
3	2.576	2.616	2.641	2.955	3.053
4	2.522	2.568	2.569	2.613	2.617

Although a rather limited dataset, the correlation between the average of the four closest atoms (the values in the above table are each for two atoms) and the segregation energy is very strong, as shown in the graph below.

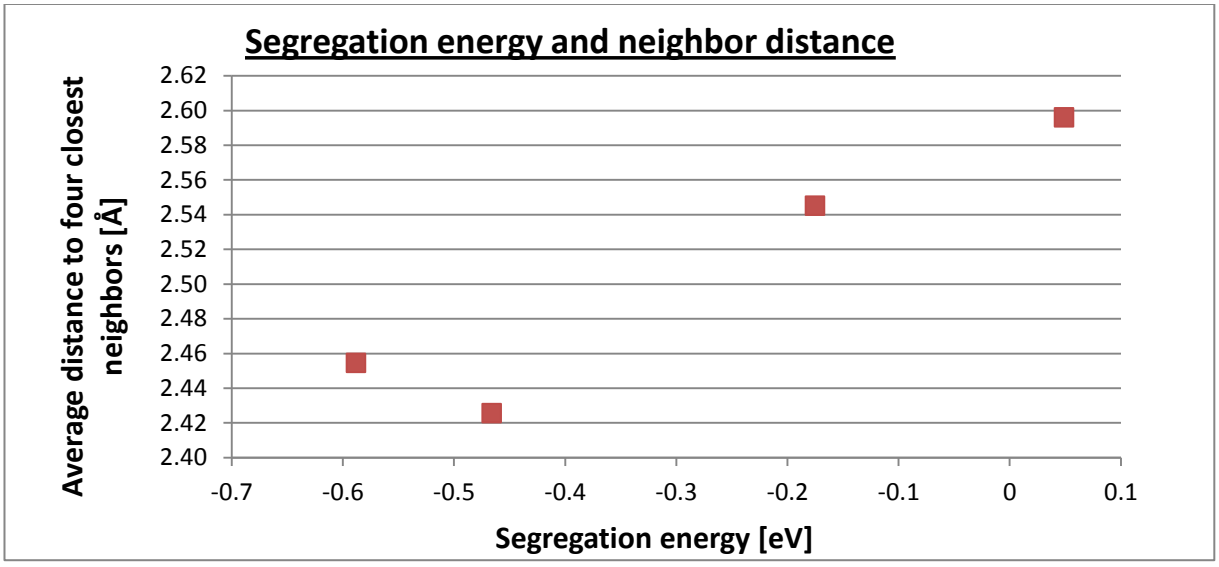

Graph 9: Correlation between segregation energy and neighbor distance

The relaxation behavior is also worthy of investigation. As already mentioned this relaxation does little to change the energy of the system, but it does affect the interatomic distances. These are shown in the table below.

Table 7: Post relaxation distances in Å

Position	Distance to closest	Distance to second closest	Distance to third closest	Distance to fourth closest	Distance to fifth closest
1	2.442	2.444	2.484	2.484	2.496
3	2.500	2.547	2.610	2.955	3.014
4	2.500	2.542	2.547	2.519	2.550

All atomic distances are reduced, clearly, a close proximity between copper and phosphorus lowers the energy of the system. Also noticeable is that all distances are reduced simultaneously, not that some distances become very small while others become very large.

Lastly, a lower limit of the optimal distance between copper and phosphorus can also be given. The relaxation of the interstitial phosphorus atom lowered the energy tremendously. It started with 7 neighbors at 0.20 nm, and after relaxation the energy is lowered by almost 2 eV/atom and the closest neighbor remains at 0.22 nm.

5.12. Accuracy of the calculations

Several remarks can be made regarding the accuracy of the calculations. These fall into two categories, errors in the calculations and the differences between the modeled system and the real system.

The errors on the calculations can be estimated from the convergence tests. Both k-point grid and cut-off energy are finite and thus introduce errors. These have been found to be of the order of 1 meV and 10 meV respectively. Other sources of numerical errors, such as rounding, are present in all calculations, including the convergence tests. Those errors are thus already included in the errors from convergence. Thus, it is a reasonable assumption that the energy of the described system is known up to 10 meV.

More can be said about the differences between the model and a real grain boundary. First, there is the approximate nature of DFT calculations. For the cohesion energy of copper, the calculated value differed 4% from the real value. This deviation seems to be somewhat systematic, so the real incurred error could be less. In any case, the performance of DFT, and this includes the accuracy of the used functional and pseudopotential, has been tested for a large number of model systems, but not for the exact system at hand. It is always possible therefore, although unlikely, that the DFT results are exceptionally bad for the studied system. This uncertainty should always be kept in mind.

A much graver concern is the finiteness of the repeat unit, which leads to all sorts of problems. First there is the fact that the grain boundaries are placed very close together, only three lattice parameters apart. The resulting influence appears to be small, as shown by the electronic structure differences in Figure 22 and by the fact that the energy of embedding a free phosphor atom in the cell (and creating a free copper atom) differed only 15 meV for the pseudobulk and true bulk. An estimate of the incurred error would thus be of this order.

The phosphorus atoms themselves will similarly interact. This is the reason why a segregant was chosen with an appreciable solubility in copper. However, this interaction will certainly be non-zero. Related to the finite concentration of phosphorus in the system is the problem with the discrete concentration jump. In this work, a comparison is made between a system with 3 % phosphorus in bulk and a system with 5 phosphorus atoms per nm^2 at the grain boundary. In reality, the segregation energy should depend on an infinitesimal concentration difference. The magnitude of these errors is virtually impossible to establish. Potentially, convergence tests could be carried out for ever larger supercells. However, the associated computational expense would quickly rise and require careful management. If the error due to the grain boundaries is any indication however, these errors should not dominate the calculated values.

Lastly, there is the question of how good the used model is. While the modified Σ9 grain boundary was indeed found to possess a high grain boundary energy, similar to random grain boundaries, it remains a special grain boundary and thus could have special properties.

Questions can also be asked about the relaxation scheme. This was apparently successful in maintaining the bulk characteristics between the grain boundaries, the fact that not all atoms could relax will also influence the calculations. However, this error is likely highly transferable. When a grain boundary was relaxed again after the introduction of a phosphorus atom, the energy difference was on the order of 3 meV, except for the interstitial case where it was several eV. Thus the atomic configuration at a grain boundary does not change much when a phosphorus atom is introduced. Subsequently, whatever influence the incomplete relaxation has on the energy of a grain boundary, this influence is likely felt in both those systems where a phosphorus atom is present in the grain boundary and those where it is not. The energies of these two systems is subtracted to find the segregation energy, thus the error will likely cancel largely out.

All in all, an estimated error of ~30 meV seems reasonable, half due to the error on calculations and half due to the interaction of the grain boundaries. This while keeping in mind of course that the modeled system is a very specific grain boundary and not a true random one. Even if another 10 meV is added for the interaction between the phosphorus atoms, although this value is rather speculative, the calculated segregation energy is still an order of magnitude greater than the error. Even when the DFT approximations are taken into account, such an error is workable.

6. Conclusion

The goal of this work was to calculate the segregation energy of an impurity in copper using Density Functional Theory calculations. It was decided to use a modified Σ9 grain boundary as a model grain boundary. To avoid excessive oversaturation, phosphorus was chosen as segregating impurity.

The segregation energy has been calculated for five sites in the grain boundary, four substitutional positions and one interstitial. For two substitutional sites a low, but noticeable segregation energy was calculated, for the other two substitutional sites the segregation energy was very low or non-existing.

The magnitude of the segregation energy was found to be closely related with the atomic configurations at the grain boundary. The sites with sizeable grain boundary segregation energy had closer copper neighbors than the other sites. As such, the intuitive concept that the smaller phosphorus ion prefers an environment where atoms are closer spaced is verified and more importantly, quantified somewhat in terms of distance and energy. Also it was found that the system lowers all copper-phosphor distances when it is allowed to relax, so it does not sacrifice some copper-phosphor interactions to optimize others. Rather, the copper-copper distances are enlarged.

The uncertainty on the calculations stems from many sources. The numerical accuracy is of the order of 10 meV. The periodicity of the system accounts for an uncertainty of at least another 15 meV. Its true impact is unknown as the interaction between the phosphorus atoms has not been assessed. Assuming that this interaction causes a deviation of the same order as the known deviations, the calculated segregation energy is still an order of magnitude larger than the uncertainty.

DFT calculations inherently introduce some errors since the method is approximate. However, there is no reason to suspect that the calculations for this system give worse results than for the model systems which have been extensively compared to the experiment. The expected deviation of several percent does not overshadow the calculated value.

Lastly, the modified Σ9 grain boundary is a special grain boundary and thus its relevance can be argued against since most grain boundaries in practice are random. However, the grain boundary was found to have a high grain boundary energy. While no guarantee in itself, it suggests at least some resemblance with random grain boundaries.

As such, the used method is fruitful and is viable for repetition. It is the hope of the author that this work describes the followed procedures and precautions adequately so that persons wishing to undertake similar calculations in the future can advance quickly.

7. Bibliography

1. G.H. Li and L.D. Zhang, *RELATIONSHIP BETWEEN MISORIENTATION AND BISMUTH INDUCED EMBRITTLEMENT OF 001 TILT BOUNDARY IN COPPER BICRYSTAL*. Scripta Metallurgica Et Materialia, 1995. **32**(9): p. 1335-1340.
2. D. Porter, Easterling, Sherif, *Phase Transformations in Metals and Alloys*. Third Edition. 2009, Boca Raton, Florida: CRC Press. p41-44.
3. W. Callister, *Materials Science and Engineering An Introduction*. 2007, U.S.A.: John Wiley & Sons, Inc. p51-60.
4. F. Humphreys, Hatherley, *Recrystallization and Related Annealing Phenomena*. Second Edition. 2004, Oxford, UK: Elsevier ltd. p12-14.
5. J. Verhoeven, *Fundamentals of Physical Metallurgy*. 1989, U.S.A.: John Wiley & Sons, Inc.
6. B. Andrew, C. Smith. [cited 2013 28 05]to be found at http://cnx.org/content/m16927.
7. J. Sietsma, *Microstructure of Materials, Course at Ghent University*. 2011.
8. Z. Lei, Z. Ying, and L. Guang-Hong, *Structure and stability of He and He-vacancy clusters at a Sigma5(310)/ 001 grain boundary in bcc Fe from first-principles.* Journal of Physics: Condensed Matter, 2013. **25**(9): p. 095001 (10 pp.)-095001 (10 pp.).
9. D. McLean, *Grain Boundaries in Metals.* Oxford University Press, 1957.
10. P. Lejcek, *Effect of solute interaction on interfacial segregation and grain boundary embrittlement in binary alloys.* Journal of Materials Science, 2013. **48**(6): p. 2574-2580.
11. Z. Shengjun, et al., *Cohesion enhancing effect of magnesium in aluminum grain boundary: a first-principles determination.* Applied Physics Letters, 2012. **100**(23): p. 231904 (4 pp.)-231904 (4 pp.).
12. D. McLean, *INFLUENCE OF SEGREGATION ON CREEP CAVITATION.* Metals Forum, 1981. **4**(1-2): p. 44-47.
13. R. Sandstrom and H.C.M. Andersson, *The effect of phosphorus on creep in copper.* Journal of Nuclear Materials, 2008. **372**(1): p. 66-75.
14. N.H. Heo, et al., *Decarburization, grain boundary segregation of P and primary water stress corrosion cracking in a low-alloy steel.* Scripta Materialia, 2008. **59**(11): p. 1200-1203.
15. W. Jian and S. Shenhua, *A unified model of grain-boundary segregation kinetics.* Journal of Applied Physics, 2011. **110**(6): p. 063531 (14 pp.)-063531 (14 pp.).
16. P. Lin *Grain Boundary Engineering for Improved Resistance to Intergranular Degredation*. 2013. Available from http://www.edax.com/download/Grain%20Boundary%20Engineering%20for%20Improved%20Resistence%20to%20Intergranular%20Degradation-1.pdf
17. F. Caestecker, *(Dutch) Nauwkeurigheidsstudie voor het ab initio berekenen van de mengingsenthalpie bij bulk metallic glasses*. 2012, Ghent University.
18. S. Cottenier, *Computational Materials Physics, course at Ghent University*. 2012.
19. S. Cottenier. *Density Functional Theory and the family of (L)APW-methods: a step-by-step introduction*. (Instituut voor Kern- en Stralingsfysica, K.U.Leuven, Belgium), 2002, ISBN 90-807215-1-4 to be found at http://www.wien2k.at/reg_user/textbooks.
20. K. Capelle, *A bird's-eye view of density-functional theory.* Brazilian Journal of Physics, 2006. **36**(4A): p. 1318-1343.
21. J.P. Perdew, K. Burke, and M. Ernzerhof, *Generalized gradient approximation made simple.* Physical Review Letters, 1996. **77**(18): p. 3865-3868.
22. Wikimedia foundation, Inc. *Pseudopotential - wikipedia, the free encyclopedia*, to be

found at http://en.wikipedia.org/wiki/Pseudopotential
23. C. Rostgard, *The Projector Augmented-wave Method.* 2009.
24. G. Kresse and J. Furthmuller, *Efficiency of ab-initio total energy calculations for metals and semiconductors using a plane-wave basis set.* Computational Materials Science, 1996. **6**(1): p. 15-50.
25. G. Kresse, M. Marsman, and J. Furthmuller. *VASP the GUIDE*. 2012 to be found at http://cms.mpi.univie.ac.at/VASP/
26. H.J. Monkhorst and J.D. Pack, *SPECIAL POINTS FOR BRILLOUIN-ZONE INTEGRATIONS.* Physical Review B, 1976. **13**(12): p. 5188-5192.
27. Wikimedia foundation, Inc. *Gibbs phenomenon - wikipedia, the free encyclopedia*, to be found at http://en.wikipedia.org/wiki/Gibbs_phenomenon
28. A.F. Wright and S.R. Atlas, *DENSITY-FUNCTIONAL CALCULATIONS FOR GRAIN-BOUNDARIES IN ALUMINUM.* Physical Review B, 1994. **50**(20): p. 15248-15260.
29. S. Ogata, et al., *Ab-initio analysis of aluminum Sigma=5 grain boundaries - Fundamental structures and effects of silicon impurity.* Computational Materials Science, 1997. **7**(3): p. 271-278.
30. S.K. Bhattacharya, et al., *Ab initio study of symmetrical tilt grain boundaries in bcc Fe: structural units, magnetic moments, interfacial bonding, local energy and local stress.* Journal of Physics-Condensed Matter, 2013. **25**(13).
31. P. Lejcek, et al., *Why calculated energies of grain boundary segregation are unreliable when segregant solubility is low.* Scripta Materialia, 2013. **68**(8): p. 547-550.
32. R.-Z. Wang, S. Tanaka, and M. Kohyama, *First-Principles Tensile Tests of Tilt and Twist Grain Boundaries in Al.* Materials Transactions, 2012. **53**(1): p. 140-146.
33. E.A. Kotomin, et al., *Ab initio modelling of UN grain boundary interfaces*, in *International Conference on Functional Materials and Nanotechnologies*. 2012.
34. C. Feng, et al., *Possible effects of oxygen in Te-rich Sigma 3 (112) grain boundaries in CdTe.* Solid State Communications, 2012. **152**(18): p. 1744-1747.
35. L. Hak-Sung, et al., *Characterization and atomic modeling of an asymmetric grain boundary.* Physical Review B (Condensed Matter and Materials Physics), 2011. **84**(19): p. 195319 (7 pp.)-195319 (7 pp.).
36. G. Ning, et al., *Multiscale modelling of bi-crystal grain boundaries in bcc iron.* Journal of Nuclear Materials, 2009. **385**(2): p. 262-7.
37. H. Sawada, *First-principles study of grain boundary embrittlement in Fe-Ni-S alloy.* Computational Materials Science, 2012. **55**: p. 17-22.
38. H.H. Kart, M. Uludogan, and T. Cagin, *DFT studies of sulfur induced stress corrosion cracking in nickel.* Computational Materials Science, 2009. **44**(4): p. 1236-1242.
39. S.H. Kim, et al., *Grain boundary character distribution and intergranular corrosion behavior in high purity aluminum.* Scripta Materialia, 2001. **44**(5): p. 835-839.
40. K.-i. Ikeda, et al., *Grain boundary structure of ultrafine grained pure copper fabricated by accumulative roll bonding.* Materials Transactions, 2008. **49**(1): p. 24-30.
41. O.H. Duparc, et al., *Atomic structures of symmetrical and asymmetrical facets in a near Sigma=9{221} tilt grain boundary in copper.* Acta Materialia, 2007. **55**(5): p. 1791-1800.
42. J.R. Hu, et al., *HRTEM investigation of the multiplicity of Sigma=9 0(1)over-bar-1 /(122) symmetric tilt grain boundary in Cu.* Materials Chemistry and Physics, 2002. **74**(3): p. 313-319.
43. K. Lejaeghere, Veronique Van Speybroeck, Guido Van Oost, Stefaan Cottenier, *(In press), Error estimates for solid-state density-functional theory predictions: an*

overview by means of the ground-state elemental crystals. http://arxiv.org/abs/1204.2733, 2013.

44. C. Kittel, *Introduction to Solid State Physics*. 8th edition. 2005: John Wiley & Sons, Inc.
45. A.Y. Lozovoi, A.T. Paxton, and M.W. Finnis, *Structural and chemical embrittlement of grain boundaries by impurities: A general theory and first-principles calculations for copper.* Physical Review B, 2006. **74**(15).
46. Grazulis, S., et al., *Crystallography Open Database (COD): an open-access collection of crystal structures and platform for world-wide collaboration.* Nucleic Acids Research, 2012. **40**(D1): p. D420-D427.

Appendix

.cif file of the modified Σ9 grain boundary

```
#======================================================================

# CRYSTAL DATA

#----------------------------------------------------------------------

data_VESTA_phase_1


_pd_phase_name                         'Cu '
_cell_length_a                         2.55582
_cell_length_b                         7.66745
_cell_length_c                         21.68682
_cell_angle_alpha                      90
_cell_angle_beta                       90
_cell_angle_gamma                      90
_symmetry_space_group_name_H-M         'P 1'
_symmetry_Int_Tables_number            1

loop_
_symmetry_equiv_pos_as_xyz
   'x, y, z'

loop_
   _atom_site_label
   _atom_site_occupancy
   _atom_site_fract_x
   _atom_site_fract_y
   _atom_site_fract_z
   _atom_site_adp_type
   _atom_site_B_iso_or_equiv
   _atom_site_type_symbol
   Cu1      1.0    -0.000000     0.111111     0.888889     Biso  1.000000 Cu
   Cu2      1.0    -0.000000     0.888889     0.611111     Biso  1.000000 Cu
   Cu3      1.0     0.500000     0.055556     0.694444     Biso  1.000000 Cu
   Cu4      1.0     0.500000     0.944444     0.805556     Biso  1.000000 Cu
   Cu5      1.0    -0.000000     0.222222     0.777778     Biso  1.000000 Cu
   Cu6      1.0    -0.000000     0.777778     0.722222     Biso  1.000000 Cu
   Cu7      1.0     0.500000     0.388889     0.861111     Biso  1.000000 Cu
   Cu8      1.0     0.500000     0.611111     0.638889     Biso  1.000000 Cu
   Cu9      1.0    -0.000000     0.555556     0.944444     Biso  1.000000 Cu
   Cu10     1.0    -0.000000     0.444444     0.555556     Biso  1.000000 Cu
   Cu11     1.0     0.000000     0.000000     0.500000     Biso  1.000000 Cu
   Cu12     1.0     0.000000     0.000000     0.000000     Biso  1.000000 Cu
   Cu13     1.0     0.500000     0.166667     0.583333     Biso  1.000000 Cu
   Cu14     1.0     0.500000     0.833333     0.916667     Biso  1.000000 Cu
   Cu15     1.0    -0.000000     0.333333     0.666667     Biso  1.000000 Cu
   Cu16     1.0    -0.000000     0.666667     0.833333     Biso  1.000000 Cu
   Cu17     1.0     0.500000     0.500000     0.750000     Biso  1.000000 Cu
   Cu18     1.0     0.500000     0.166667     0.416667     Biso  1.000000 Cu
   Cu19     1.0     0.500000     0.833333     0.083333     Biso  1.000000 Cu
   Cu20     1.0     0.000000     0.444444     0.444444     Biso  1.000000 Cu
   Cu21     1.0    -0.000000     0.555556     0.055556     Biso  1.000000 Cu
   Cu22     1.0     0.500000     0.722222     0.472222     Biso  1.000000 Cu
   Cu23     1.0     0.500000     0.277778     0.027778     Biso  1.000000 Cu
   Cu24     1.0     0.500000     0.055556     0.305556     Biso  1.000000 Cu
   Cu25     1.0     0.500000     0.944444     0.194444     Biso  1.000000 Cu
   Cu26     1.0     0.000000     0.333333     0.333333     Biso  1.000000 Cu
   Cu27     1.0    -0.000000     0.666667     0.166667     Biso  1.000000 Cu
   Cu28     1.0     0.500000     0.611111     0.361111     Biso  1.000000 Cu
   Cu29     1.0     0.500000     0.388889     0.138889     Biso  1.000000 Cu
   Cu30     1.0    -0.000000     0.888889     0.388889     Biso  1.000000 Cu
   Cu31     1.0     0.000000     0.111111     0.111111     Biso  1.000000 Cu
   Cu32     1.0     0.000000     0.222222     0.222222     Biso  1.000000 Cu
   Cu33     1.0    -0.000000     0.777778     0.277778     Biso  1.000000 Cu
   Cu34     1.0     0.500000     0.500000     0.250000     Biso  1.000000 Cu
```

Matlab script to construct grain boundary supercells

```
function [s] = boundary()

%XMAX, YMAX, ZMAX: supercell dimensions in terms of conventional cell, respectively a,b,c-axis
XMAX = 1/sqrt(2)
YMAX = sqrt(9/2)
ZMAX = 3

%theta: half the relative rotation of the two grain boundaries, will be performed around a-axis
theta = atan(sqrt(2)/4)

%orientation of supercell (in conventional cell unit row vectors) rotation will be done around a-axis, concatenation on c-axis
%note: this is in terms of the conventional cell *after* rotation (as is usually given in literature)
a=[1,1,0];
b=[-1,1,4];
c=[2,-2,1];
A=transpose([a./norm(a);b./norm(b);c./norm(c)]);

%for relaxation: factor for change in z-axis (1=no relaxation)
factr = 0.9778

%path: where the structfile can be found and where it will be saved
pth = 'Cu.struct'
savepth = strcat(num2str(10000*factr),'.struct')

%atoms with this c-coordinate (+- 0.0001) will be removed from half-cells (-1=no effect)
zdelete = 0.055555

%END OF PARAMETERS

%Creation of half cells
s1=rotate(XMAX,YMAX,ZMAX,0,A,pth);
s2=rotate(XMAX,YMAX,ZMAX,2*theta,A,pth);
%Deletion of atoms specified by zdelete
s1=makespace(s1,zdelete);
s2=makespace(s2,zdelete);
%Change of c-axis. Atoms are moved symmetrically away or to grain boundary, atoms with c-coordinate 0 in halfcells do not move
s1=enlarge(s1,factr);
s2=enlarge(s2,factr);
%Concatenation of halfcells
s1=displace(s1);
s=mergestruct(s2,s1);
%Saving of completed cell
savestruct(s,savepth,0);
end

function [struct2]=makespace(struct,zdelete)
struct2=struct;
for i=[1:struct.nat] %check all atoms in struct, remove them from struct2 if zdelete criterion matches
  if abs(struct.pos(i,3)-zdelete)<=10^(-4)
    struct2=rmatom(struct,i);
  end
end
end

function [struct]=enlarge(struct,factr)
%modify c-axis with factr, vacuum is added (or substracted) from top
struct=rescale_c_2(struct,factr*struct.a(3));
%check all atoms in struct, move them if c-coordinate is different from 0
for i=[1:struct.nat]
  if  struct.pos(i,3)~=0
    struct.pos(i,3)=struct.pos(i,3)+(factr-1)/2/factr;
  end
end
end

function [struct]=displace(struct)
%double c-axis, vacuum is added on top
struct=rescale_c_2(struct,2*struct.a(3));
%move all atoms half a cell up
 for i=[1:struct.nat]
  struct.pos(i,3)=struct.pos(i,3)+0.5;
end
end
```

```
function [werk]=rotate(XMAX,YMAX,ZMAX,theta,A,pth)

%For rounding errors
smallnumber=10^(-8)

%Loading of the structures, makeprimitive for brlat, conventional is used for supercell size, remove symmetry
primitive=makeprimitive(loadstruct(pth));
werk=makeconventional(loadstruct(pth));
werk.lattic='P';

%Rotate brlat
ROT = [1, 0, 0; 0, cos(theta), sin(theta); 0, -sin(theta), cos(theta)]*inv(A);
werk.brlat=transpose(ROT*transpose(primitive.brlat));

%Supercell construction in cartesian coordinates: x,y,z vectors contain supercell axis in cartesian coordinates
werk.a(1)=werk.a(1).*XMAX;
werk.a(2)=werk.a(2).*YMAX;
werk.a(3)=werk.a(3).*ZMAX;
werk.lat2car(1,:)=werk.lat2car(1,:).*XMAX;
werk.lat2car(2,:)=werk.lat2car(2,:).*YMAX;
werk.lat2car(3,:)=werk.lat2car(3,:).*ZMAX;
x=werk.lat2car(1,:);
y=werk.lat2car(2,:);
z=werk.lat2car(3,:);

%Rotating initial positions
for i = [1:primitive.nat]
  primitive.pos(i,:)=transpose(ROT*transpose(primitive.pos(1,:)));
end

% supercell expressed in brlat (brlat is given is cartesian coordinates)
a=werk.brlat(1,:);
b=werk.brlat(2,:);
c=werk.brlat(3,:);
supc=[a;b;c]*inv([x;y;z]);
invabc=inv([a;b;c]);

% upper and lower parameters for iteration (huge influence on runtime, stricter limits should be possible)
% currently: coordinates in brlat vectors of corner diagonally from origin (depends on supercell geometry)
r = 1/norm(supc(1,:))+1/norm(supc(2,:))+1/norm(supc(3,:))+1
amin=-r; amax=r; bmin=-r; bmax=r; cmin=-r; cmax=r;

%remove all atoms in werk, so that the new ones can be added
for i = [1:werk.nat]
  werk=rmatom(werk,1);
end

%add new atoms to werk lattice
for j = [1:primitive.nat]
 atomicnumber=primitive.zz(j);
 currentpos=primitive.pos(j,:);
 for o = [floor(amin):ceil(amax)];
  for p = [floor(bmin):ceil(bmax)];
   for q = [floor(cmin):ceil(cmax)];
    pos=[o,p,q]-currentpos*invabc;      %substract starting position (received in cartesian) from pos (expressed in brlat)
    indices=pos*supc;                   %convert position in brlat to position in supercell coordinates
    for i =[1:3]                        %Rounding errors: set slightly negative values to zero
     if indices(i)<0 && indices(i)>-smallnumber
      indices(i)=0;
     end
    end
    %if all three supercell coordinates lie between 0 and 1, add atom to supercell
    if indices(1) >= 0 && indices(2) >=0 && indices (3) >= 0 && indices(1) < 1-smallnumber && indices (2) < 1-smallnumber &&
indices(3) < 1-smallnumber
      werk=addatom(werk,atomicnumber,indices,0);
    end

   end
  end
 end

end
end
```

Matlab script to perform Birch-Murnaghan fit

```
% fun is an anonymous function that describes a Birch-Murnaghan fit from X
% to Y

% The fitting parameters in the vector b are: E V B B' in that order

fun = @(b,X) b(1)+9/16*b(2)*b(3).*(((b(2)./X(:)).^(2/3)-1).^3.*b(4)+((b(2)./X(:)).^(2/3)-
1).^2.*(6-4.*(b(2)./X(:)).^(2/3)))

%Lattice scaling factors from POSCAR
X=[
0.96;0.97;0.98;0.99;1;1.01;1.02;1.03;1.04;1.001;1.002;1.003;1.004;1.005;1.006;1.007;1.008;1.00
9]
%Cube for volume scaling
X=X.^3
%Multiply with volume of unit cell
X=X.*1.80723505711^3*2

%Calculated energies
Y=[ -3.604406;-3.652762;-3.68724;-3.709318;-3.720318;-3.721489;-3.713932;-3.69862;-3.676438;-
3.720863;-3.721301;-3.721651;-3.721903;-3.722062;-3.722129;-3.722097;-3.721985;-3.721781]

%Initial guess
b0 = [-3.72; 12; 0.8; 5.3]
X
%Nonlinear regression, store parameters in b
b = nlinfit(X,Y, fun, b0)
```

Script to submit jobs

```
#!/bin/bash
#By Michael Sluydts 14/12/2011
#Edited 08.05.2013

if [ $1 -gt 0 ]; then
        walltime=$[$1-1]':59:00'
else
        walltime='0:10:00'
fi

if [ $1 -gt 12 ]; then
        queue='long'
elif [ $1 -gt 1 ]; then
        queue='short'
else
        queue='debug'
fi

#Ask all memory on haunter, gastly and gengar

memstring=""
if [ "$VSC_INSTITUTE_CLUSTER" == "haunter" ] || [ "$VSC_INSITUTE_CLUSTER" == "gastly" ]; then
  memstring=$'#PBS -l vmem=31gb\nexportI_MPI_FABRICS=dapl'
else
  memstring='#PBS -l vmem=36533mb'
fi

dir=`pwd`
cat > submit.sh << !
#!/bin/bash
#PBS -N ${dir:35}
#PBS -V
#PBS -m e
#PBS -q $queue
#PBS -l walltime=$walltime
#PBS -l nodes=$2:ppn=all
$memstring
module purge

export VSC_INSTITUTE_CLUSTER=$VSC_INSTITUTE_CLUSTER
ulimit -s unlimited

module load cluster
module load jobs
module swap scripts/3.0.0
module load VASP/5.3.3-ictce-4.1.13-mt

newgrp g_vasp5

cd $dir

free -m
date

mympirun --output $dir/tempout vasp

free -m
date

exit 0
!

qsub submit.sh
```